# MEIG1/PACRG associated and non-associated functions of axonemal dynein light intermediate polypeptide 1 (DNALI1) in mammalian spermatogenesis

Yi Tian Yap [1,*], Wei Li [1,*], Qian Huang [1,2,*], Qi Zhou [1,2], David Zhang [3], Ljljiana Mladenovic-Lucas [4], James G Granneman [4], David C Williams Jr[5], Rex A Hess [6], Aminata Touré [7], Zhibing Zhang [1,8]

1. Department of Physiology, Wayne State University School of Medicine, Detroit, MI, 48201.
2. Department of Occupational and Environmental Medicine, School of Public Health, Wuhan University of Science and Technology, Wuhan, Hubei, 430060, China.
3. College of William and Mary, Williamsburg, VA, 23187, USA.
4. Center for Molecular Medicine and Genetics, Wayne State University School of Medicine, Detroit, MI, 48201, USA.
5. Department of Pathology and Laboratory Medicine, University of North Carolina, Chapel Hill, NC 27599.
6. Department of Comparative Biosciences, College of Veterinary Medicine, University of Illinois, 2001S. Lincoln, Urbana, IL 61802-6199.
7. Institut pour l'avancée des Biosciences, Université Grenoble Alpes, INSERM U1209, CNRS UMR 5309, F-38000 GRENOBLE, France.
8. The C.S. Mott Center for Human Growth and Development, Department of Obstetrics & Gynecology, Wayne State University, Detroit, MI, 48201.

* These authors contributed equally in this study.

Address correspondence to: Zhibing Zhang, MD, PhD

Associate Professor

Department of Physiology

Wayne State University

275 E Hancock Street

Detroit, MI, 48201

Email: gn6075@wayne.edu

**Keywords:** DNALI1; manchette; cargo transport; spermiogenesis.

## Summary statement

Axonemal dynein light intermediate polypeptide 1 (DNALI1) is required for sperm formation and male fertility. It associates with the MEIG1/PACRG complex in the manchette and is involved in a cargo transport system. In addition, it might be related to IFT and sperm individualization.

## Abstract

Axonemal dynein light intermediate polypeptide 1 (DNALI1) was originally cloned from *Chlamydomonas reinhardtii* in an effort to find motor proteins essential for flagellar motility. Here we report that DNALI1 is a binding partner of parkin co-regulated gene 1 (PACRG), which forms a complex with meiosis expressed gene 1 (MEIG1) in the manchette, a transient and unique structure only present in the elongating spermatids and required for normal

spermiogenesis of the male germ cell differentiation process. DNALI1 recruits the PACRG protein in transfected CHO cells, and also stabilizes PACRG in bacteria and transfected mammalian cells. The untagged DNALI1 could also be co-purified with His-tagged PACRG in the gel filtration assay. Immunofluorescence staining on isolated male germ cells revealed that DNALI1 was present in the manchette of elongating spermatids, and colocalized with PACRG in this structure. In *Pacrg* mutant mice, localization of DNALI1 in the manchette was not changed, suggesting that DNALI1 and PACRG form a complex in the manchette, with DNALI1 being an upstream molecule. Mice deficiency in DNALI1 specifically in male germ cells showed dramatically reduced sperm numbers and were infertile. In addition, majority of the sperm exhibited abnormal morphology including misshapen heads, bent tails and enlarged midpiece, discontinuous accessory structure, and loss of sperm individualization, emphasizing the importance of DNALI1 in sperm development. Examination of testis histology revealed impaired spermiogenesis in the conditional *Dnali1* knockout mice. Electron microscopy revealed disrupted ultrastructure in sperm of the *Dnali1* mutant mice. Testicular levels of MEIG1, PACRG and SPAG16L proteins were not changed in the *Dnali1* mutant mice. However, MEIG1 and SPAG16L were no longer present in the manchette in the absence of DNALI1. These findings demonstrate that DNALI1 is involved in the connection of the MEIG1/PACRG complex to carry cargo proteins along the manchette microtubules for sperm flagella formation. Given that *Dnali1* mutant mice showed impaired sperm individualization that was not observed in the MEIG1 nor PACRG-deficient mice, DNALI1 might fulfill other

63 functions beyond its role associated with the MEIG1/PACRG complex. Thus, DNALI1 plays
64 multiple roles in sperm cell differentiation and function.
65
66 **Introduction**
67 Motile cilia are microtubule-based organelles with a core "9 + 2" axonemal structure (1).
68 They generate fluid flow by their beating in various epithelia and also enable sperm cell
69 progression, which overall confers vital functions in eukaryotes (2, 3). In humans, motile cilia
70 dysfunction results in multiple syndromes, including bronchiectasis, impaired mucociliary
71 clearance, chronic cough, sinusitis, and male infertility, which are described as immotile cilia
72 syndrome, as well as *primary ciliary dyskinesia* (PCD) (4, 5). Ciliary beat is driven by dynein
73 motor protein complexes, associated with the inner and outer dynein arms of axonemal
74 ultrastructure, which are anchored to the peripheral axonemal microtubules. The heavy,
75 medium and light chains constitute the dynein motors, and each chain has a different molecular
76 weight and provides an important function (6, 7). Hence, in mammals the loss of dynein
77 function leads to PCD with ciliary impairment with hydrocephalus, body axis asymmetry, and
78 male infertility (2, 8, 9).
79 Human axonemal dynein light intermediate polypeptide 1 (*DNALI1*) is the homolog of
80 the *Chlamydomonas* inner dynein arm gene *p28*, an important component of the ciliated
81 dynamic arm, which is mainly responsible for cilium movement (10, 11). The molecular
82 analysis of *DNALI1 (*human *hp28*) gene was revealed by Dr. Shalender Bhasin's laboratory
83 more than 20 years ago. The gene was localized on chromosome 1 region p35.1, and *DNALI1*

84 transcripts were detected in several ciliated structures, including sperm flagella, suggesting that
85 this gene could be a good candidate for patients suffering from immotile cilia syndrome (11).
86 In addition to PCD, *DNALI1* was also related to a variety of diseases, including Frontotemporal
87 Lobar Degeneration (FTLD), Diploid Breast Carcinoma (DPC), Osteosarcoma (OS), Allergic
88 Rhinitis (AR), Nasopharyngeal Carcinoma (NPC), and Alzheimer's disease (AD) (12-18),
89 although the precise mechanisms are unclear. However, the role of *DNALI1* in human male
90 reproduction has not been investigated.

91 Recently, *Dnali1* was identified as a sex-related gene involved in spermatogenesis of
92 several fishes, including the Odontobutis potamophila, the Ussuri catfish Pseudobagrus
93 ussuriensis, and the olive flounder Paralichthys olivaceus (19-21). The expression of *Dnali1*
94 showed sexually dimorphism with predominant expression in the testis. This suggested that the
95 fish *Dnali1* might play an important role in the testis, especially in the period of
96 spermatogenesis (21). Sajid et al. cloned the murine *Dnali1* with significant similarity to the
97 *p28* gene of *Chlamydomonas reinharditii* and to *DNALI1* (*hp28*) gene (22). The murine *Dnali1*
98 gene is localized on chromosome 4 and consists of six exons. It has two transcripts and is
99 expressed in several tissues, but the strongest expression was observed in testis. During the
100 first wave of spermatogenesis, both *Dnali1* mRNA and protein were dramatically increased
101 during the spermiogenesis phase, which corresponds to spermatid cell differentiation.
102 Immunofluorescence studies demonstrated that DNALI1 was detected in spermatocytes and
103 abundant in round and elongated spermatids. Moreover, the DNALI1 protein was localized in

104 flagella of mature sperm (22), indicating that *Dnali1* may play an essential role in mouse sperm
105 formation and male fertility.

106 Sperm production and formation is a complex process consisting of mitosis, meiosis and
107 finally spermiogenesis (23). During spermiogenesis, germ cells undergo dramatic changes with
108 the formation of sperm-unique structures, including the flagellum (24). Many genes have been
109 described to precisely regulate these morphologic changes (25). We previously discovered that
110 mouse meiosis-expressed gene 1 (MEIG1) and Parkin co-regulated gene (PACRG) form a
111 protein complex in the manchette, a transient microtubule structure localized in the head
112 compartment of sperm cells during differentiation. It was demonstrated that this protein
113 complex controls sperm flagellum formation, with PACRG being an upstream molecule of
114 MEIG1 (26-29). The MEIG1/PACRG complex was shown to function as part of the cargo
115 transport system, called intra-manchette transport system (IMT) (30), which transports sperm
116 flagella proteins, including SPAG16, for sperm tail assembly. However, how the
117 MEIG1/PACRG complex associates with the axonemal motor system for cargo transport
118 remained unclear.

119 Using mouse PACRG as bait for a yeast two-hybrid screen, DNALI1 was identified as a
120 protein binding-partner. To investigate the function of DNALI1, a *Dnali1* conditional knock-
121 out mouse model was generated using a floxed *Dnali1* mouse line, which was crossed with
122 *Stra8*-iCre transgenic mice, to specifically disrupt the *Dnali1* gene in the male germ cells.
123 Reported here, the *Dnali1* conditional knockout (*Dnali1* cKO) mice have significantly reduced
124 sperm number and are infertile. In addition, the majority of sperm exhibited abnormal

125 morphology, strongly indicating the importance of *Dnali1* in the development of sperm flagella.
126 Importantly, in the conditional *Dnali1* mutant spermatid germ cells, MEIG1 and SPAG16L
127 were not present in the manchette, indicating that DNALI1 is required for MEIG1/PACRG
128 complex localization and for transport of cargo proteins to assemble the sperm flagellum. Some
129 unique phenotypes discovered in the *Dnali1* mutant mice but not in the MEIG1 and PACRG-
130 deficient mice suggest additional roles of the gene in sperm cell differentiation.
131
132 **Materials and methods**
133 **Ethics statement**
134 All animal research was executed in compliance with the guidelines of the Wayne State
135 University Institutional Animal Care with the Program Advisory Committee (Protocol number:
136 18-02-0534).
137
138 **Yeast two-hybrid experiments**
139 Full-length mouse PACRG coding sequence was amplified using the following primers:
140 forward: 5'-GAATTCATGCCGAAGAGGACTAAACTG-3'; reverse: 5'-
141 GGATCCGTCAGTTCAGCAAGCACGACTC-3'. After TA cloning and sequencing, the
142 correct cDNA was subcloned into the EcoR1/BamH1 sites of pGBKT7, which was used to
143 screen a Mate & Plate™ Library-Universal Mouse (Normalized) (Clontech, Mountainview,
144 CA; Cat#: 630482) using the stringent protocol according to the manufacturer's instructions.
145 For direct yeast two-hybrid assay, the coding sequence of the DNALI1 cDNA was amplified

by RT-PCR using the following primers: forward: 5'-GAATTCATGATACCCCCAGCAGACTCTCTG-3' and reverse: 5'-GGATCCGATCACTTCTTCGGTGCGATAATGCC-3'. The correct cDNA was cloned into EcoRI/BamH1 sites of pGAD-T7 vector. The yeast was transformed with the indicated plasmids using the Matchmaker™ Yeast Transformation System 2 (Clontech, Cat#: 630439). Two plasmids containing simian virus (SV) 40 large T antigen (LgT) in pGADT7 and p53 in pGBKT7 were co-transformed into AH109 as a positive control. The AH109 transformants were streaked out in complete drop-out medium (SCM) lacking tryptophan, leucine and histidine to test for histidine prototrophy.

**Localization assay**

To generate mouse PACRG/pEGFP-$N_2$ plasmid, *Pacrg* cDNA was amplified using the primer set: forward: 5'-GAATTCATGCCGAAGAGGACTAAACTG-3; reverse: 5'-GGATCCGGTTCAGCAAGCACGACTC-3', and the correct *Pacrg* cDNA was ligated into the pEGFP-$N_2$ vector. To generate mouse DNALI1/Flag construct, *Dnali1* cDNA was amplified using the primer set: forward: 5'-GAATTCAATGATACCCCCAGCAGACTCTCTG-3'; reverse: 5'-CTCGAGTCACTTCTTCGGTGCGATAATGCC-3', and the correct *Dnali1* cDNA was ligated into the pCS3+FLT vector. The PACRG/pEGFP-$N_2$ and DNALI1/Flag were transfected individually or together into CHO cells by using Lipofectamine™ 2000 transfection reagent (Invitrogen, Waltham, MA). The CHO cells were cultured with DMEM (with 10% fetal bovine

167 serum) at 37°C. After 48 h transfection, the CHO cells were processed for immunofluorescence
168 with an anti-Flag antibody.
169
170 **Co-immunoprecipitation assay**
171 Mouse *Pacrg* cDNA was amplified using the following primers: forward; 5'-
172 GAATTCACCAGACAAGATGCCGAAGAGG-3'; reverse: 5'-
173 TCTAGAGGTCAGTTCAGCAAGCACGACTC-3', and the correct *Pacrg* cDNA was ligated
174 into the pCS2+MT vector to create the PACRG/Myc plasmid. The PACRG /Myc and
175 DNALI1/Flag plasmids were co-transfected into COS-1 cells by sing Lipofectamine™ 2000
176 transfection reagent (Invitrogen). After 48 h transfection, the cells were processed for co-
177 immunoprecipitation assay. For co-immunoprecipitation assays, the cells were lysed with IP
178 buffer (Beyotime, Jiangsu, China; Cat No. P0013) for 5 min and centrifuged at 10,000 g for
179 3~5 min. The supernatant was pre-cleaned with protein A beads at 4°C for 30 min, and the pre-
180 cleared lysate was then incubated with anti-MYC antibodies at 4°C for 2 h. The mixture was
181 then incubated with protein A beads at 4°C overnight. The beads were washed with IP buffer
182 three times and then re-suspended in 2x Laemmli sample buffer and heated at 95°C for 5 min.
183 The samples were centrifuged at 3,000 g for 30 s, and the supernatant was then subjected to
184 Western blot analysis with MYC and Flag antibodies.
185
186 **Gel filtration experiments**

187 Full-length mouse *Pacrg* cDNA (amplified by a forward primer: 5'-
188 GAATTCGGTGCCGCGCGGCAGCATGCCGAAGAGGACTAAACTG-3' and a reverse
189 primer: 5'-GTCGACTCAGTTCAGCAAGCACGACTC-3') was cloned into the upstream
190 multiple clone site of the dual expression vector pCDFDuet-1 to create the
191 PACRG/pCDFDuet-1 plasmid, and the translated protein was tagged with hexahistidine. The
192 full-length mouse *Dnali1* cDNA (amplified by a forward primer: 5'-
193 GATATCGATGATACCCCCAGCAGACTCTC-3' and a reverse primer: 5'-
194 CTCGAGTCACTTCTTCGGTGCGATAATG-3') was inserted into the downstream multiple
195 cloning site to create the PACRG/DNALI1/pCDFDuet-1 plasmid. The dual expression plasmid
196 was transformed into the Rosetta II (DE3) (Invitrogen) E. coli strain, grown in Luria Bertani
197 medium, and induced with 1 mM isopropyl-β-d-thiogalactopyranoside at an A600 ~ 0.8 for
198 2 hours. The bacterial pellets from 1 L of growth media were resuspended in 30 mL of B-PER
199 reagent (Thermo Scientific, Waltham, MA), and expressed proteins were purified from the lysis
200 supernatant by Nickel affinity and gel filtration (Superdex 75 26/60, GE Healthcare, Chicago,
201 IL) chromatography. The purified protein was concentrated and passed over the gel filtration
202 column a second time before Western blot analysis.

203

204 **Luciferase complementation assay**

205 HEK293 cells were grown in 12-well plates and transfected in triplicate with N- and C-
206 luciferase fragments (supplied by Dr. James G Granneman, Wayne State University) fused to
207 mouse PACRG and DNALI1 along with various controls as specified in the figure legends.

The following primers were used to create the constructs: PACRG/C-Luc forward: 5'-AAGCTTCGATGGTGAAGCTAGCTGCCAAATG-3', PACRG/C-Luc reverse: 5'-ACCGGTGGCACCAGGGTATGGAATATGTCCAC-3', N-Luc/DNALI1 forward: 5'-AAGCTTATGGCAGAGTTGGGCCTAAATGAG-3', N-Luc/DNALI1 reverse: 5'-ACCGGTGGATCTTCAGATTCATATTTTGCCAG-3'. After transfection, cells were cultured for 24 h. Luciferase activities were measured as described previously (31) and readings were recorded using Veritas microplate luminometer. Experiments were performed three times independently, and the results are presented with standard errors.

**Western blot analysis**

Tissue samples were collected from 3-4-month-old mice, and tissue extracts were obtained after lysis with buffer containing 50 mM Tris–HCl pH 8.0, 170 mM NaCl, 1% NP40, 5 mM EDTA, 1 mM DTT and protease inhibitors (Complete mini; Roche diagnostics GmbH, Basel, Switzerland). Protein concentration for lysates was determined using BCA reagent (Sigma-Aldrich, St. Louis, MO), and equal amounts of protein (50 μg/lane) were heated to 95°C for 10 min in sample buffer, loaded onto 10% sodium dodecyl sulfate-polyacrylamide gels, separated with electrophoresis, and transferred to polyvinylidene difluoride membranes (Millipore Corporation, Bedford, MA). Membranes were blocked (Tris-buffered saline solution containing 5% nonfat dry milk and 0.05% Tween 20 [TBST]) and then incubated with the indicated primary antibodies at 4°C overnight. After being washed in TBST, the blots were incubated with immunoglobulin conjugated to horseradish peroxidase for 1 h at room

229 temperature. After washing, the target proteins were detected with Super Signal
230 chemiluminescent substrate (Pierce, Thermo Scientific). The following primary antibodies
231 were used: anti-His (1: 2000, Cat No: 70796-4, Novagen, Madison, WI); anti-DNALI1 (1:
232 10,000 for Proteintech 17601-1-AP, Rosemont, IL; and 1:2000 for Abcam, Cambridge, UK,
233 Cat No: ab87075. This antibody has been discontinued); anti-GFP (1: 1000, Cat No:
234 11814460001, Roche); anti-MYC (1: 2000, Cat No: C-19 Sc788, Santa Cruz, Dallas, TX); and
235 β-ACTIN (1: 2000, Cat No: 4967S, Cell Signaling Technology, Danvers, MA). Secondary
236 antibodies include anti-Rabbit IgG (1: 2,000, Cat No: 711166152, Jackson ImmunoResearch,
237 West Grove, PA) and anti-Mouse IgG (1: 2,000, Cat No: DI-2488, Vector Laboratories,
238 Burlingame, CA). Each Western blot was performed using three independent biological
239 replicates.
240
241 **Preparation of testicular cells and immunofluorescence analysis**
242 Testes were separated from 3-4-month-old mice and incubated in a 15mL centrifuge tube with
243 5mL DMEM containing 0.5 mg/mL collagenase IV and 1.0 μg/mL DNase I (Sigma-Aldrich)
244 for 30 min at 32°C and shaken gently. Then the testes were washed once with PBS after
245 centrifugation at 1,000 rpm for 5 min under 4°C, and the supernatant was discarded. Afterwards,
246 the cell pellet was fixed with 5 mL paraformaldehyde containing 0.1 M sucrose and shaken
247 gently for 15 min at room temperature. After washing three times with PBS, the cell pellet was
248 re-suspended with 2 mL PBS and loaded on positively charged slides. The slides were stored
249 in a wet box at room temperature after air drying. Then, the spermatogenic cells were

250 permeabilized with 0.1% Triton X-100 (Sigma-Aldrich) for 5 min at 37◦C. Finally, the samples
251 were incubated overnight with primary antibodies (Anti-DNALI1: 1: 100, Abcam, Cat No:
252 ab87075; Anti-PACRG: 1: 200, generated by our laboratory; Anti-α-tubulin, 1:200, Sigma, Cat
253 No: T9026-2mL; Anti-MEIG1, 1:400, generated by our laboratory; Anti-SPAG16L, 1: 200,
254 generated by our laboratory; anti-DYNC1H1: 1: 100, Santa Cruz Biotechnology, Cat No: sc-
255 7527). After washing three times with PBS, the slides were incubated with secondary
256 antibodies for 1h at room temperature. CyTM3 AffiniPure F (ab')2 Fragment Donkey Anti-
257 Rabbit IgG (H + L) (1: 200, Jackson ImmunoResearch, Cat No: 711166152) and DyLight 488
258 Horse Anti-Mouse IgG Antibody (1: 400, Vector Laboratories，Cat No: DI-2488) are two
259 secondary antibodies used in this experiment. Images were captured using multiple
260 microscopes in separate locations: confocal laser scanning microscopy (Zeiss LSM 700,
261 Virginia Commonwealth University), Olympus IX-81 microscope equipped with a spinning-
262 disc confocal unit (Dr. James G. Granneman, Wayne State University), and Nikon DS-Fi2
263 Eclipse 90i Motorized Upright Fluorescence Microscope (The C.S. Mott Center for Human
264 Growth and Development, Department of Obstetrics & Gynecology, Wayne State University).
265
266 **Generation of *Dnali1* conditional knockout (cKO) mice**
267 *Dnali1*$^{flox/flox}$ mice were generated at the Center for Mouse Genome Modification at University
268 of Connecticut, and *Stra8-iCre* mice were purchased from the Jackson Laboratory (Stock No:
269 008208). Cre recombinase was shown to be only active in male germ cells (32). To generate
270 the germ cell-specific *Dnali1* cKO mouse model, 3-4-month-old Stra8-cre males were crossed

271 with 3-4-month-old *Dnali1*$^{flox/flox}$ females to obtain *Stra8-iCre*; *Dnali1*$^{flox/+}$ mice. The 3-4-
272 month-old *Stra8-iCre*; *Dnali1*$^{flox/+}$ males were crossed back with 3-4-month-old *Dnali1*$^{flox/flox}$
273 females again. The *Stra8-iCre*; *Dnali1*$^{flox/flox}$ were considered to be the homozygous cKO mice,
274 and *Stra8-iCre*; *Dnali1*$^{flox/+}$ mice were used as the controls. Genomic DNA was isolated to
275 genotype the offspring. The following primers were used for genotyping: *Stra8-iCre* forward:
276 5′-GTGCAAGCTGAACAACAGGA-3′; *Stra8-iCre* reverse: 5′-
277 AGGGACACAGCATTGGAGTC-3′. An 844 bp PCR product is amplified from the floxed
278 allele of the *Dnali1* with the following primers: forward: 5′-
279 CCTGTGGGAAAGCTAACCCAGC-3'(DliScF5), and reverse: 5′-
280 GCTGGGGATGCGGTGGGCTC -3′ (BGHpAr). A 129 bp PCR product is amplified from the
281 wild-type allele using the following primers: forward:
282 5'- GACAGGGATGGAGGTTGGGAG-3', and reverse: 5'-
283 GAATGAGTGGTCAGGCCTCTG-3'. The *Pacrg* mutant mice were purchased from Jackson
284 Laboratory (stock number: 000567, 27).
285
286 **Assessment of male fertility and fecundity**
287 Sexually mature *Dnali1* cKO and control male mice were each mated with a 2-4-month old
288 wild-type female for at least 2 months. The presence of vaginal plugs was checked, and the
289 pregnancy of females was recorded. The number of pups was counted the day after birth.
290 Average litter sizes are presented as the number of total pups born divided by the number of
291 mating cages.

292

293 **Sperm parameters**

294 After breeding studies, the male mice were euthanized by cervical dislocation following
295 anesthesia. Sperm were collected after swimming out from the cauda epididymis in 37°C PBS.
296 Cells were counted using a hemocytometer chamber under a light microscope, and sperm
297 number was calculated by standard methods. Motility percentages and velocities (average path
298 velocity) were then analyzed using Image J (National Institutes of Health, Bethesda, MD) and
299 the plug-in MTrackJ.

300

301 **HE staining of testis and epididymis sections**

302 Testes and epididymides of adult mice were collected and fixed in 4% paraformaldehyde (PFA)
303 in phosphate-buffered saline (PBS) at 4°C overnight. The tissues were embedded in paraffin,
304 sectioned at 5μm thickness, deparaffined, and stained with hematoxylin and eosin using
305 standard procedures. Slides were examined using a BX51 Olympus microscope (Olympus
306 Corp., Melville, NY, Center Valley, PA), and photographs were taken with a ProgRes C14
307 camera (Jenoptik Laser, Germany).

308

309 **Transmission electron microscopy**

310 Mouse testes and sperm from adult control and *Dnali1* cKO mice were collected after
311 swimming out from the cauda epididymis in 37°C PBS solution followed by centrifugation at
312 1,000 × g for 10 min under 4°C and re-suspended in fixation buffer (0.2M HEPES, 8mM $CaCl_2$,

313 8% PFA, 10% Glutaraldehyde, PH7.4). Electron microscopy was performed using the method
314 described previously (33).
315
316 **Statistical analysis**
317 Statistical analyses were performed using Student's *t* test. *$p < 0.05$ was considered as
318 significant. Graphs were created using Microsoft Excel.
319
320 **Results**
321 **DNALI1 is a binding partner of PACRG**
322 PACRG, a major spermatogenesis regulator, was used as bait for a yeast two-hybrid screen.
323 The sequencing results of positive clones revealed that MEIG1 was the major binding partner
324 as previously described (26). In addition, DNALI1 encoding clones were identified multiple
325 times (**Supplemental Table 1**). A direct yeast two-hybrid assay was conducted to confirm the
326 interaction between PACRG and DNALI1. Like the positive control, the yeast co-transformed
327 with the two plasmids expressing DNALI1 and PACRG grew on the selection medium (**Figure**
328 **1A**), indicating that the two proteins interact in yeast. To further examine interaction of the two
329 proteins, CHO cells were transfected with the plasmids expressing the two proteins. When the
330 CHO cells expressed PACRG/GFP only, the protein was present in the cytoplasm (**Figure 1B,**
331 **a**) while DNALI1/FLAG was present as a vesicle located on one side of the nucleus (**Figure**
332 **1B, b**). When CHO cells expressed both proteins, PACRG/GFP was present as a vesicle and
333 was co-localized with DNALI1/FLAG (**Figure 1Bc-e**). In addition, we transfected COS-1 cells

334 with DNALI1/FLAG and PACRG/Myc expression plasmids and conducted a co-
335 immunoprecipitation assay. The MYC antibody pulled down both the Myc-tagged 28 kDa
336 PACRG and Flag-tagged 34 kDa DNALI1 proteins, suggesting an interaction between these
337 proteins (**Figure 1C**). Finally, interaction between DNALI1 and PACRG was examined by
338 luciferase complementation assay. We observed that HEK cells co-expressing PACRG/C-Luc
339 and N-Luc/DNALI1 showed robust luciferase activity, while the cells expressing either
340 PACRG/C-Luc or N-Luc/DNALI1 only showed baseline activity (**Figure 1D**).

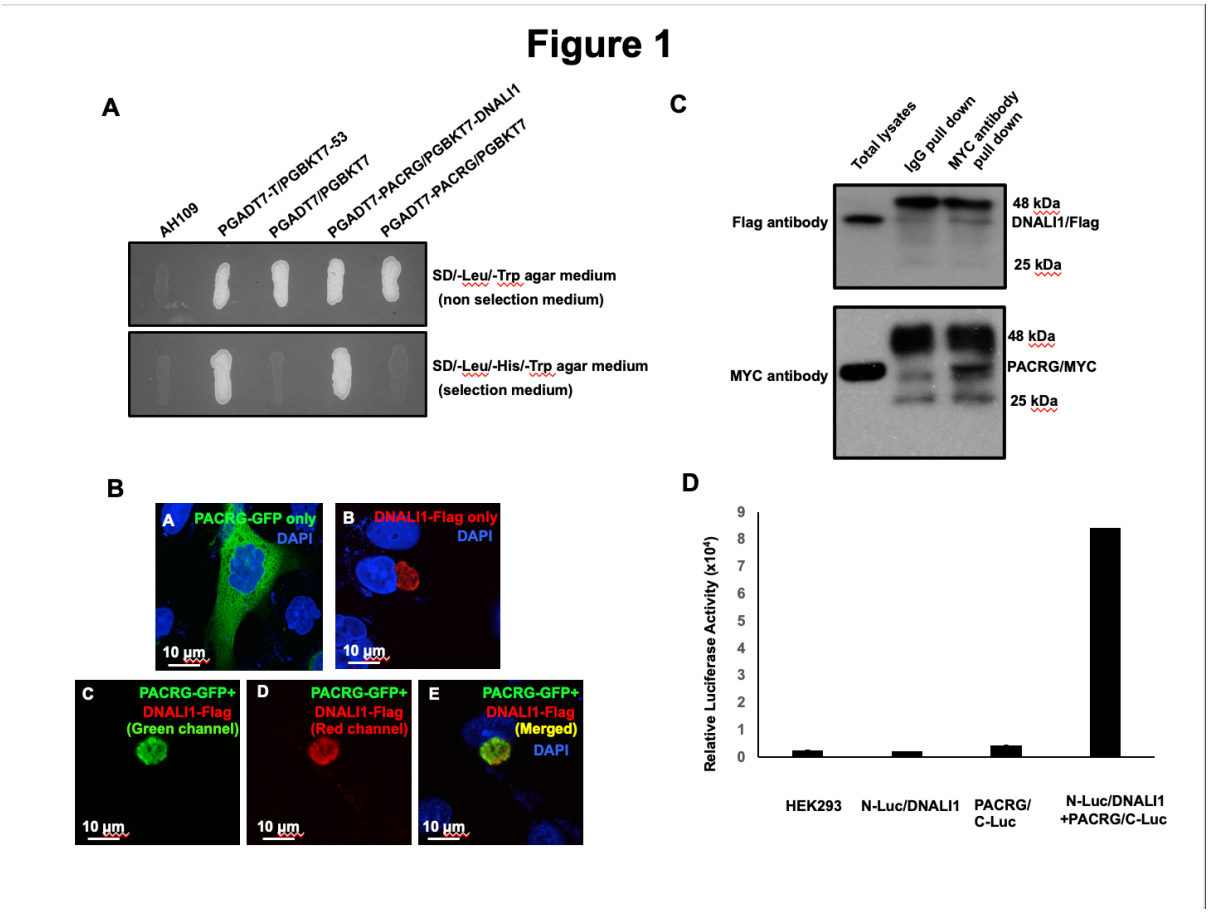


341

342 **Figure 1. DNALI1 associates with PACRG, a major spermatogenesis regulator.**

343 A. Direct yeast two-hybrid assay to examine the interaction between PACRG and DNALI1.
344 Pairs of indicated plasmids were co-transformed into AH109 yeast, and the transformed yeast
345 were grown on either selection plates (lacking leucine, histidine and tryptophan) or non-

346 selection plates (lacking leucine and tryptophan). Notice that all the yeast except AH109 grew
347 on the non-selection plate. Yeast expressing PACRG/DNALI1 and P53/large T antigen pairs
348 grew on selection plate.
349 B. DNALI1 co-localizes with PACRG in CHO cells. When expressed alone, PACRG/GFP was
350 present in the cytoplasm, and DNALI1/FLAG as a vesicle located closed to the nucleus. When
351 the two proteins were co-expressed, PACRG/GFP was present as a vesicle and co-localized
352 with DNALI1/FLAG. (Images taken with confocal laser scanning microscopy (Zeiss LSM
353 700), Virginia Commonwealth University)
354 C. Co-immunoprecipitation of DNALI1/FLAG with PACRG/Myc. COS-1 cells were
355 transfected with plasmids to co-express DNALI1/FLAG and PACRG /Myc. The cell lysate
356 was immunoprecipitated with anti-MYC antibody and then analyzed by Western blotting with
357 anti-MYC and anti-FLAG antibodies. The cell lysate immunoprecipitated with a mouse normal
358 IgG was used as a control. The anti-MYC antibody pulled down both PACRG/MYC and
359 DNALI1/FLAG.
360 D. Interaction of PACRG with DNALI1 in HEK293 cells as determined by G. princeps
361 luciferase complementation assay. HEK293 cells were transfected with the indicated plasmids,
362 and luciferase activity was evaluated 24 h after transfection. The cells expressing both N-
363 Luc/DNALI1 and PACRG/C-Luc reconstituted activity.
364
365 **DNALI1 is co-purified with His-tag PACRG when the two proteins are co-expressed in**
366 **BL21 bacteria**

In order to examine the association between DNALI1 and PACRG in bacteria, we co-expressed DNALI1 and His-tagged PACRG in BL21 cells, and a gel filtration experiment was conducted to purify the His-tagged PACRG protein into continuous fractions. Detection of His-tagged PACRG and DNALI1 proteins in the eluted fractions was examined by Western blot using specific antibodies. In line with the above interaction data, DNALI1 protein was co-purified with PACRG protein in the same fractions (**Figure 2**).

## Figure 2

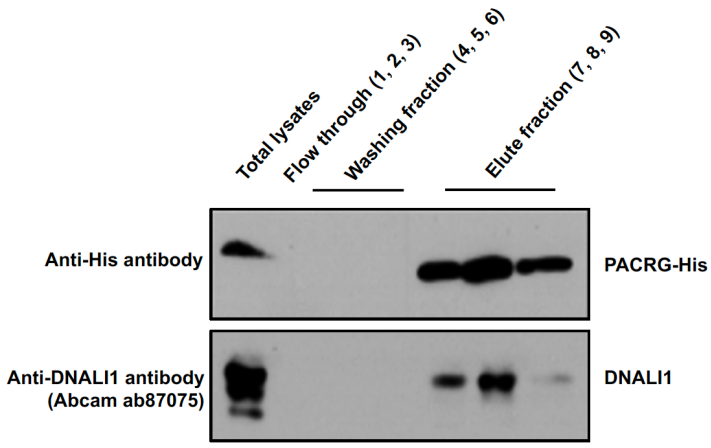


**Figure 2. Co-purification of DNALI1 with His-tagged PACRG from bacteria lysates expressing the two proteins.**

His-tagged PACRG and DNALI1 were co-expressed in BL21 bacteria and His-tagged PACRG was purified from the bacteria lysates by gel filtration experiments, and presence of the His-tagged PACRG and non-tagged DNALI1 in the fractions were examined by western blot analysis. Notice that the DNALI1 protein was present in the same fractions of His-tagged PACRG, indicating that the two proteins associate in the bacteria lysates.

**DNALI1 stabilizes PACRG in mammalian cells and bacteria.**

Functional association between PACRG and DNALI1 was further supported by the fact that DNALI1 stabilized PACRG in mammalian cells and bacteria. PACRG alone was not stable in the transfected COS-1 cells with very low protein amount detected (27). Co-expression of DNALI1 dramatically increased PACRG level (**Figure 3A**). In BL21 bacteria, no PACRG protein was detectable when the less sensitive Pico system was used for Western blot analysis when the bacteria were transformed with PACRG/pCDFDuet-1 plasmid and induced by IPTG. However, the PACRG protein was indeed expressed as it was detectable when the higher sensitive Femto system was used for Western blot analysis. When the BL21 bacteria were transformed by PACRG/DNALI1/pCDFDuet-1 plasmid so that both PACRG and DNALI1 were expressed, the PACRG was easily detectable with the Pico system (**Figure 3B**), indicating that wild-type DNALI1 also stabilized PACRG protein in bacteria.

# Figure 3

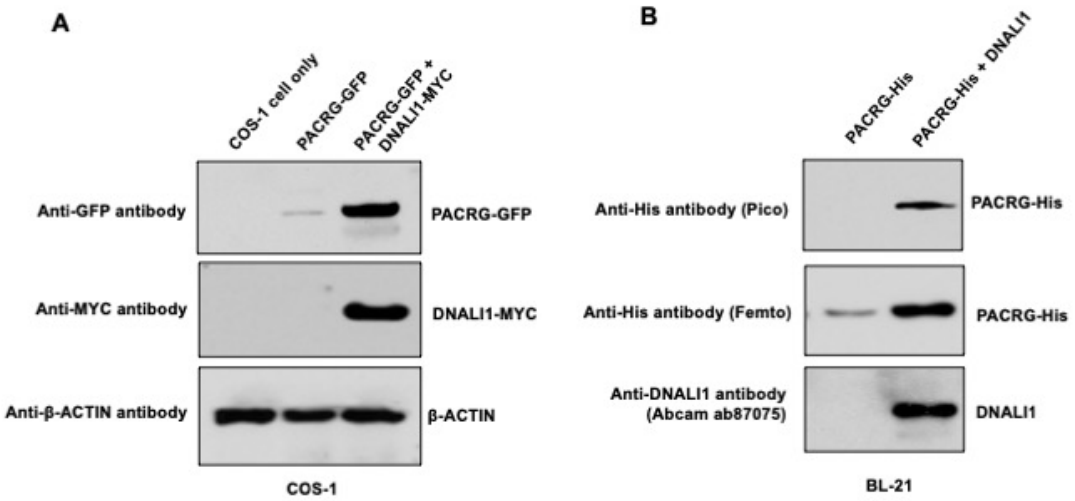


394

395 **Figure 3. DNALI11 stabilizes PACRG in mammalian cells and bacteria.**

396 A. DNALI1 stabilizes PACRG in COS-1 cells. Mouse PACRG-GFP expression is increased

397 when DNALI1 is co-expressed in transfected COS-1 cells in transient expression experiment.

398 B. DNALI1 stabilizes PACRG in bacteria. Notice that PACRG was only detectable by the high

399 sensitivity Femto system in Western blot analysis when the bacteria were transformed with

400 PACRG/pCDFDuet-1 plasmid. However, when the bacteria were transformed with

401 PACRG/DNALI1/pCDFDuet-1 plasmid to express DNALI1 protein, PACRG was also

402 detectable by less sensitive Pico system.

403

404 **Localization of DNALI1 in the manchette is not dependent on PACRG**

405 DNALI1 localization in germ cells was examined by immunofluorescence staining. In
406 elongating spermatids, DNALI1 co-localized with the α-tubulin, a manchette marker. Double
407 staining with an anti-DNALI1 polyclonal antibody and an anti-PACRG monoclonal antibody
408 revealed that the two proteins also co-localized (**Figure 4**). In *Pacrg* mutant mice, DNALI1
409 was still present in the manchette, indicating that the localization of DNALI1 in the manchette
410 is not dependent on PACRG (**Supplemental Figure 1).**

## Figure 4

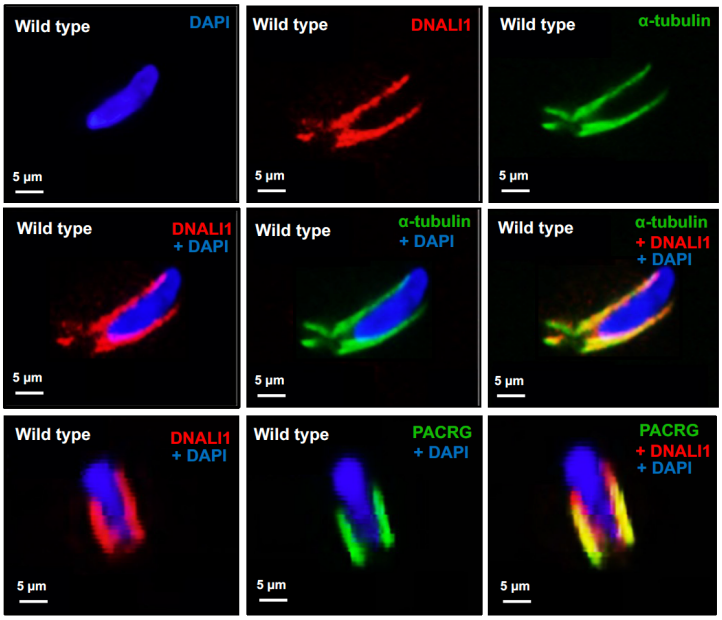


411

412 **Figure 4. Localization of DNALI1 in male germ cells of wild-type mice.**

413 Localization of DNALI1 in isolated germ cells was examined by immunofluorescence staining.
414 DNALI1 protein localizes with α-tubulin, a manchette marker in elongating spermatids (top
415 and middle panels). PACRG also co-localized with DNALI1 in the elongating spermatids
416 (bottom panel). DNALI1 seems to be closer to the nuclear membrane, and PACRG is on the
417 surface of DNALI1. (Images taken with confocal laser scanning microscopy (Zeiss LSM 700),
418 Virginia Commonwealth University)

**Inactivation of mouse *Dnali1* gene resulted in infertility associated with significantly reduced sperm number, motility and increased abnormal.**

To explore the role of DNALI1 in spermatogenesis and male fertility, a floxed *Dnali1* line was generated and the floxed *Dnali1* mice were crossed with *Stra8-Cre* mice so that the *Dnali1* gene was specifically disrupted in male germ cells (*Dnali1* cKO). Genotyping using specific primer sets indicated that homozygous mutant mice were obtained (**Supplemental Figure 2**). Examination of total testicular DNALI1 protein expression by Western blot revealed that DNALI1 was almost absent in the conditional knockout mice (**Figure 5A**). Homozygous mutant mice did not show any gross abnormalities. To test fertility of these mutant mice, 2-3-month-old controls and homozygous mutant males were bred with 2-3-month-old wild-type females for 2 months. All the control mice, including wild-type and heterozygous males, were fertile. All homozygous mutant males examined were infertile (**Figure 5B**). Epididymal sperm number, motility and morphology from the control and homozygous mutant mice were examined. The sperm count and motility was dramatically reduced in the mutant mice (**Figure 5C, D, E and Supplemental Figure 3**). Sperm from the control mice showed normal morphology (**Figure 6A**). Multiple abnormalities in sperm were observed in the mutant mice, including head defects, uneven thickness of tails and sperm bundles lacking separation (also called individualization or disengagement) (**Figure 6B-F, Supplemental Figure 4**).

# Figure 5

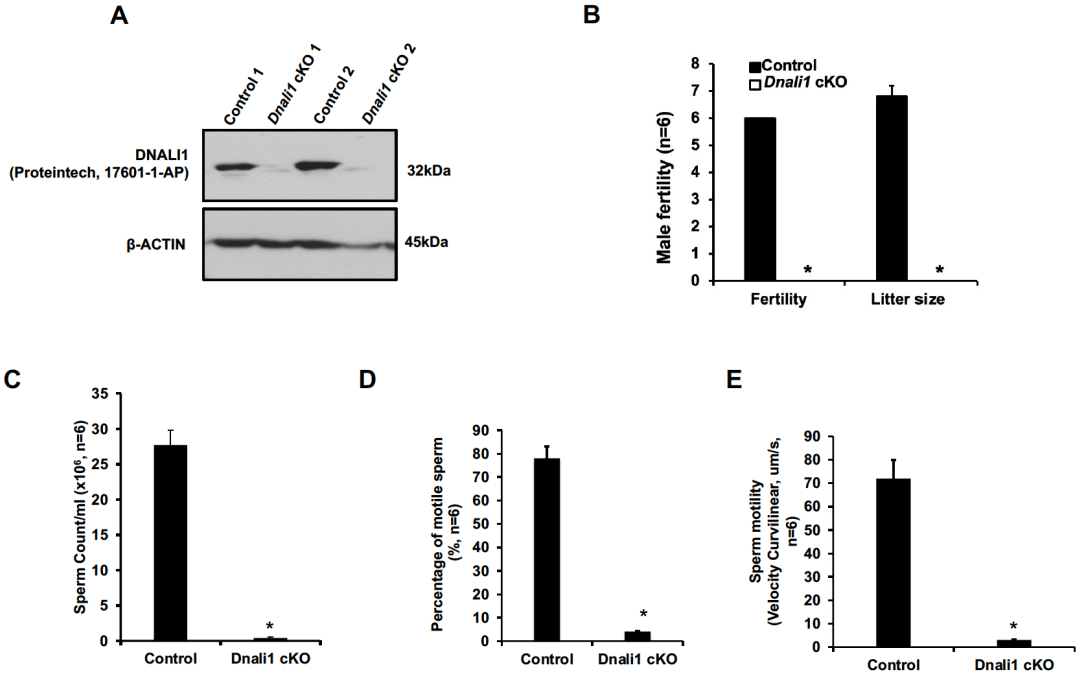


**Figure 5. Male germ cell-specific *Dnali1* knockout (*Dnali1* cKO) mice were infertile associated with significantly reduced sperm number and motility.**

A. Representative Western blot result showing that DNALI1 protein was almost absent in the testis of *Dnali1* cKO mice.

B. Male fertility of control and *Dnali1* mutant mice. Six controls and six *Dnali1* cKO mice were examined. Fertility and litter size were recorded for each mating. Notice that all mutant males were infertile.

C. Sperm count was significantly reduced in the *Dnali1* cKO mice (n=6).

D. Percentage of motile sperm in the control and *Dnali1* cKO mice (n=6).

E. Sperm motility was significantly reduced in the *Dnali1* cKO mice (n=6). Statistically significant differences: *$p < 0.05$.

## Figure 6

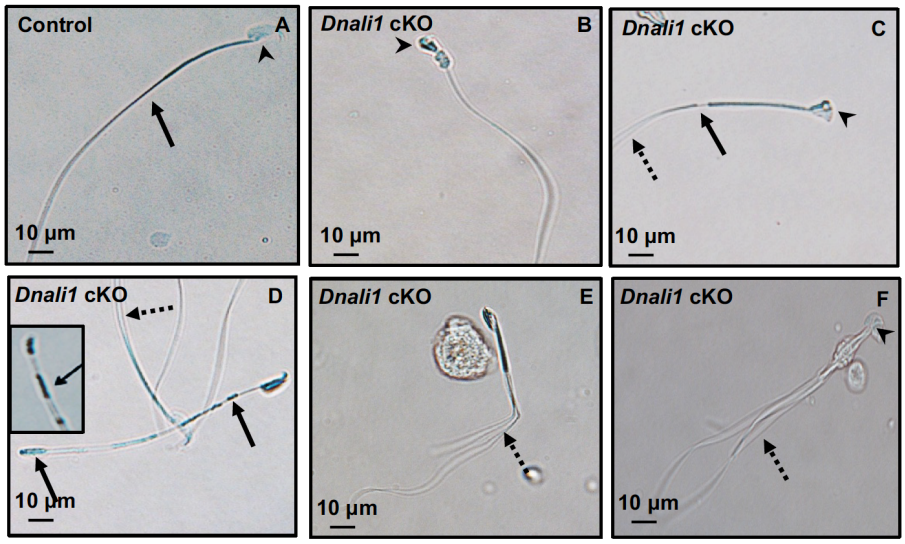


**Figure 6. Abnormal sperm morphologies in the *Dnali1* cKO mice.**

Representative epididymal sperm of control (A) and *Dnali1* cKO mice (B-F) examined by DIC microscopy. Sperm in the control mice showed normal head (A, arrowhead) and flagella (A, arrow). Multiple abnormalities were observed in the *Dnali1* cKO mice, including distorted heads (B, C and F, arrowheads), uneven thickness tails (C, D, arrows). Some sperm showed multiple flagella (C, D, E, F, dashed arrows).

**Spermatogenesis was affected in the *Dnali1* cKO mice.**

Reduced epididymal sperm number and aberrant sperm morphology in *Dnali1* cKO mice suggests impaired spermatogenesis. Therefore, histology of the testes and epididymides in adult control and *Dnali1* mutant mice was examined. In control mice, the seminiferous tubule epithelium showed elongated spermatid heads embedded as bundles among the round spermatids and developing tails extending into the lumen in stages I-III (**Figure 7Aa**). *Dnali1*

cKO mice exhibited abnormal elongating spermatid heads with compressed shapes and failure to form elongated bundles. Round spermatids were seen sloughing abnormally into the lumen in stages I-III (**Figure 7Ab and c**). In stage XII, the control seminiferous tubule epithelium showed step 12 elongating spermatid bundles with large pachytene spermatocytes in meiotic division (**Figure 7Ad**). However, in the *Dnali1* cKO mice, stage XII showed abnormal elongating spermatid heads without normal bundle formation. Additionally, the phagocytosis of thin heads of step 16 spermatids was present in the epithelium, which is evidence of spermiation failure (**Figure 7Ae and f**). Numerous mature sperm were concentrated in the cauda epididymis of control mice (**Figure 7B**, **left**). In *Dnali1* cKO mice, the cauda epididymal lumen contained fewer sperm, along with abnormal sperm heads and tails and sloughed round spermatids **(Figure 7B**, **right**).

## Figure 7

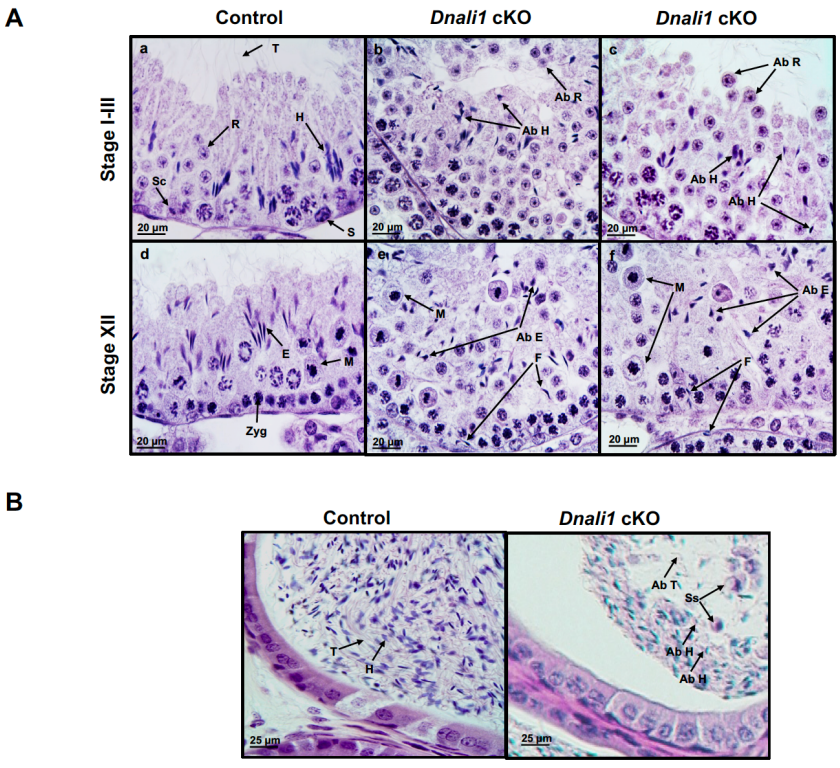

**Figure 7. Histology analysis for the adult control and *Dnali1* cKO mice.**

A. Histological evaluation of testes from control and *Dnali1* cKO mice, with selected images from Stages I-III (a-c) and Stages XII (d-f). a) Control testis seminiferous tubule epithelium showing elongated spermatid heads (H) embedded as bundles among the round spermatids (R) and developing tails (T) extending into the lumen. Sc, Sertoli cell; S, spermatogonia. b-c) *Dnali1* cKO with abnormal elongating spermatid heads (Ab H) with compressed shapes and failure to form elongated bundles. Round spermatids are seen sloughing abnormally into the lumen (Ab R). d) Control showing step 12 elongating spermatid bundles (E) with large pachytene spermatocytes in meiotic division (M). Zygotene spermatocyte, Zyg. e-f) *Dnali1* cKO with abnormal elongating spermatid heads (Ab E) without normal bundle formation. There is evidence of failure of spermiation (F), as phagocytosis of thin heads of step 16 spermatids are also present in the epithelium. Normal meiotic figures (M) are present in Stage XII.

B. Representative histology of epididymis. The control cauda epididymis shows the lumen filled with normal sperm heads (H) and tails (T). In the *Dnali1* cKO male, the cauda epididymal lumen contains numerous sperm with abnormal heads (Ab H) and tails (Ab T) and sloughed round spermatids (Ss).

**Ultrastructural changes in the seminiferous tubules of the *Dnali1* cKO mice.**

To investigate the structural basis for the molecular changes observed in the absence of DNALI1, the seminiferous tubule and cauda epididymal sperm ultrastructure was examined.

In control mice, the nuclei have normal elongated shapes with condensed chromatin (**Figure 8A**), and the flagellum contains a normal "9 + 2" axoneme structure surrounded by accessory structures, including the mitochondrial sheath (**Figure 8B**) and a fibrous sheath (**Figure 8C**). In *Dnali1* cKO mice, abnormal shapes of the nuclei were frequently seen (**Figure 8D)** and retained cytoplasmic components (not fully resorbed as part of the residual body) were present in the developed sperm (**Figure 8E, Supplemental Figure 5A).** Importantly, the two longitudinal columns were usually not associated with microtubule doublets 3 and 8, and the two semi-circumferential ribs showed defective or asymmetric formation in the principal piece of flagella; some sperm also had abnormal cell membranes (**Figure 8F, Supplemental Figure 5B, C**). Lastly, in some sperm the core "9+2" axoneme was incomplete or disorganized (**Figure 8G-I).**

**Figure 8**

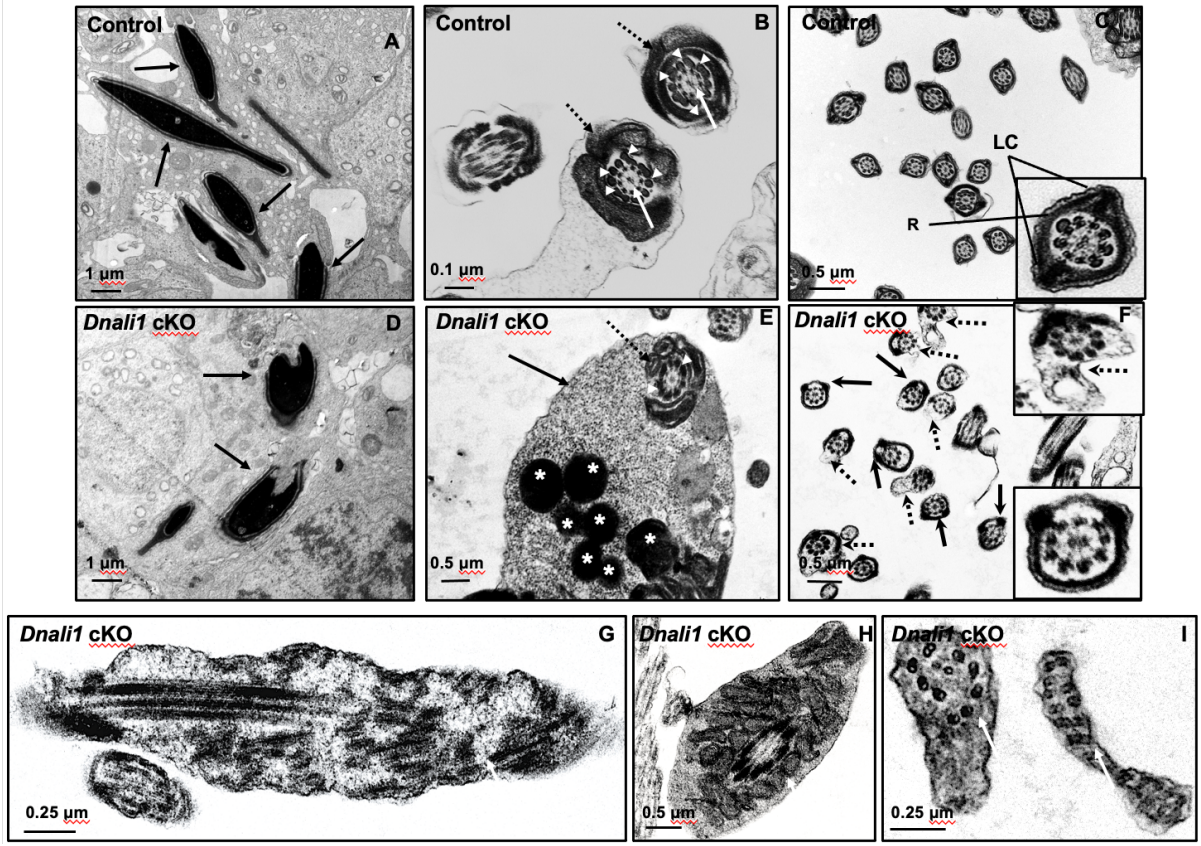

**Figure 8. Ultra-structural changes of testicular sperm of control and *Dnali1* cKO mice.**

The ultrastructure of testicular sperm from the control (A, B and C) and *Dnali1* cKO (D-I) mice were analyzed by TEM. A. Control testis seminiferous tubule epithelium showing nuclei with normally condensed chromatin (arrows). B. Control mouse showed the normal middle piece of flagella with normal "9 + 2" axoneme structure in the center (white arrows) surrounded by mitochondrial sheath (black dotted arrows) and ODF (white arrow heads). C. Normal principal piece of flagella from a control mouse, which is characterized by the presence of a complete fibrous sheath surrounding the axoneme. The fibrous sheath consists of two longitudinal columns (LC) connected by semicircumferential ribs (R). The two longitudinal columns are associated with microtubule doublets 3 and 8 with the two semicircumferential ribs are symmetrical. D. Abnormally condensed chromatin in the *Dnali1* cKO mouse (black arrows). E. A representative image of the middle piece in a flagellum from a *Dnali1* cKO mouse. The ODF (white arrow heads) and mitochondrial sheath (black dotted arrow) were present, but cytoplasm residue (black arrow) remained with a number of the lysosomes inside (white stars). F. The flagella show disorganized fibrous sheath structure in the *Dnali1* cKO mouse. Noticed that the two longitudinal columns are not associated with microtubule doublets 3 and 8 in some flagella, and the two semicircumferential ribs showing defective or asymmetric organization (black arrows and the lower, right insert); some flagella also have disrupted membranes (dashed arrows and upper, right insert). G-I: the flagella show disrupted axoneme in the *Dnali1* cKO mice (white arrows).

**Inactivation of *Dnali1* in male germ cells did not change protein levels but changed the localization of the downstream proteins.**

To examine if the loss of DNALI1 in male germ cells affected protein levels of MEIG1, PACRG and SPAG16L, Western blotting was conducted using the testis lysates of control and *Dnali1* cKO mice. There was no significant difference in protein levels of MEIG1, PACRG and SPAG16L between the control and *Dnali1* cKO mice (**Figure 9A**). Localization of MEIG1 and SPAG16L was further examined. MEIG1 was present in the cell bodies of spermatocytes and round spermatids of control mice, and protein localization was not changed in the two cell types in *Dnali1* cKO mice (27, 29, **Figure 9B**). Similarly, SPAG16L was present in the cytoplasm of spermatocytes and round spermatids in both control and *Dnali1* cKO mice (27, 29, **Figure 9C**). In contrast, while MEIG1 and SPAG16L were present in elongating spermatids of *Dnali1* cKO mice, they did not co-localized in the manchette as observed for control mice (**Figure 9D, Supplemental Figure 6**).

## Figure 9A

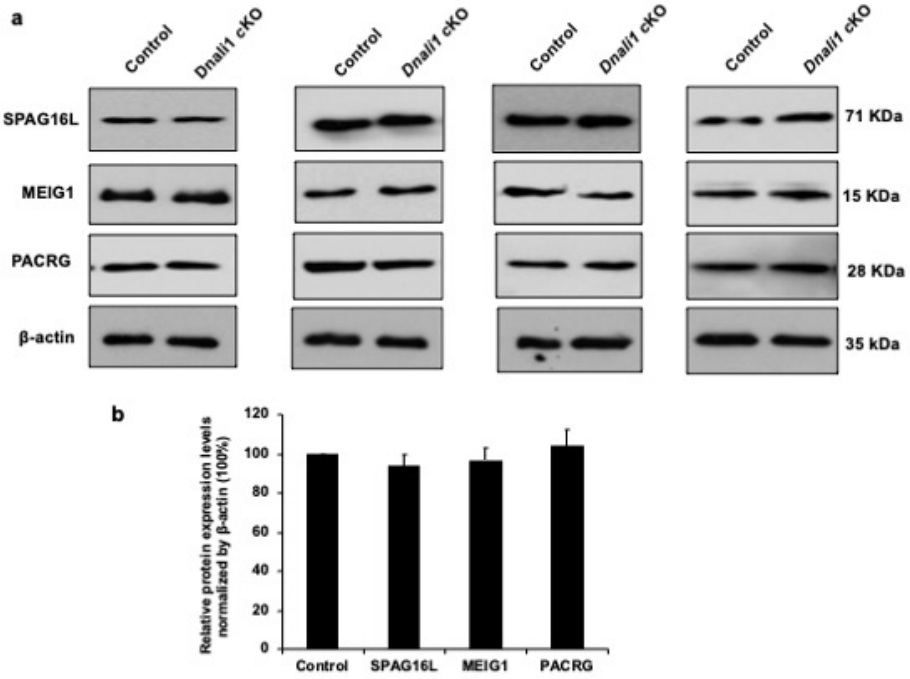


544

## Figure 9B

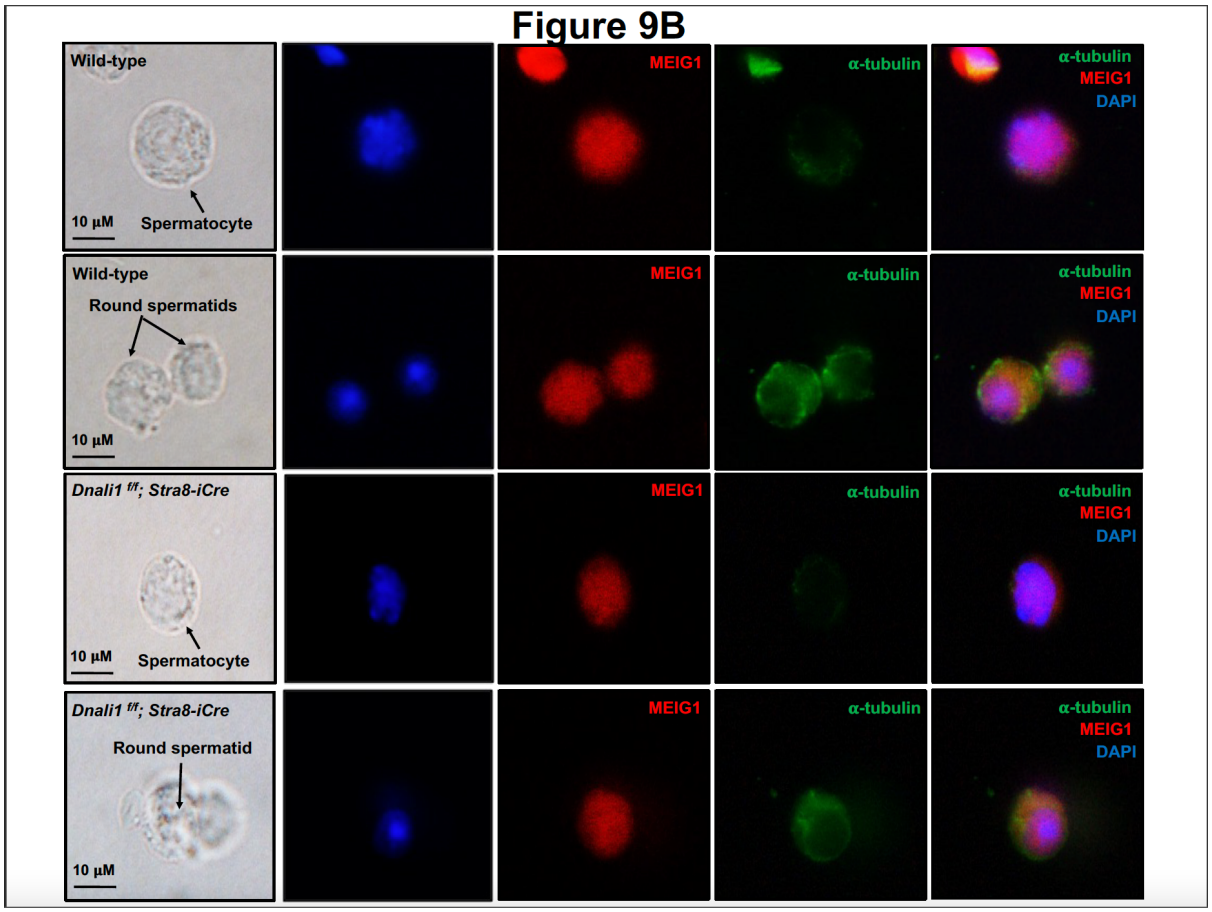


545

## Figure 9C

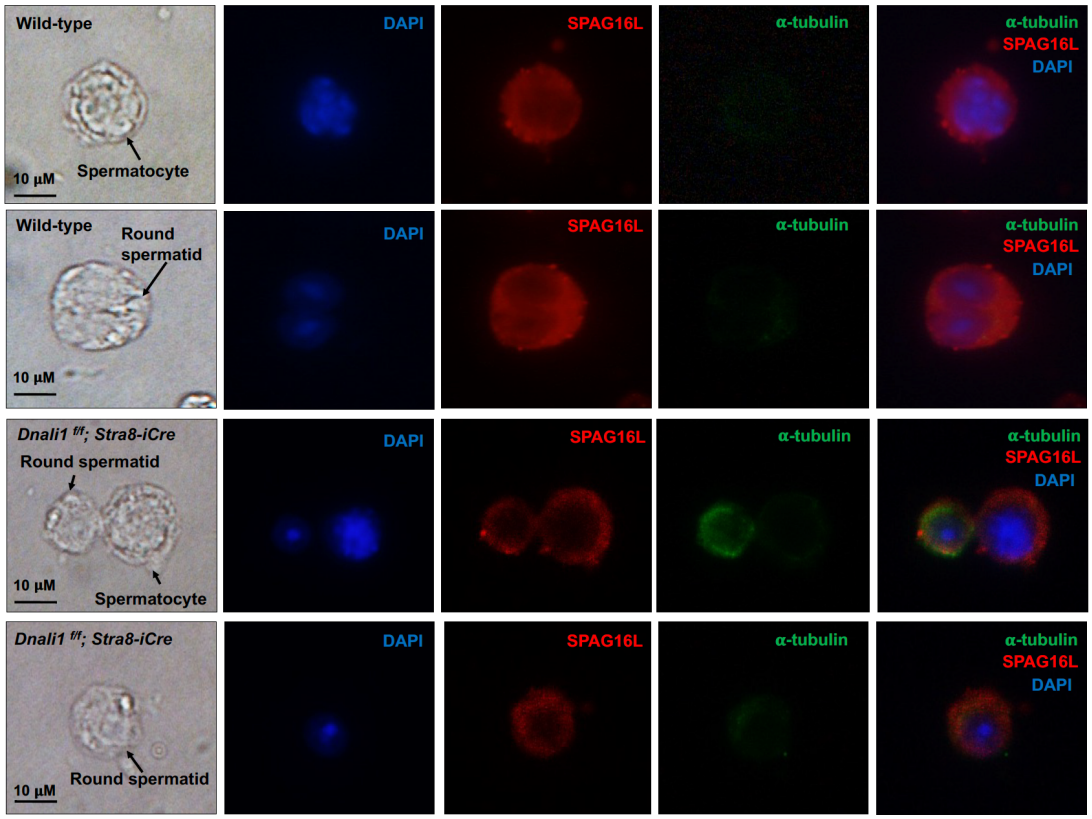


546

## Figure 9D

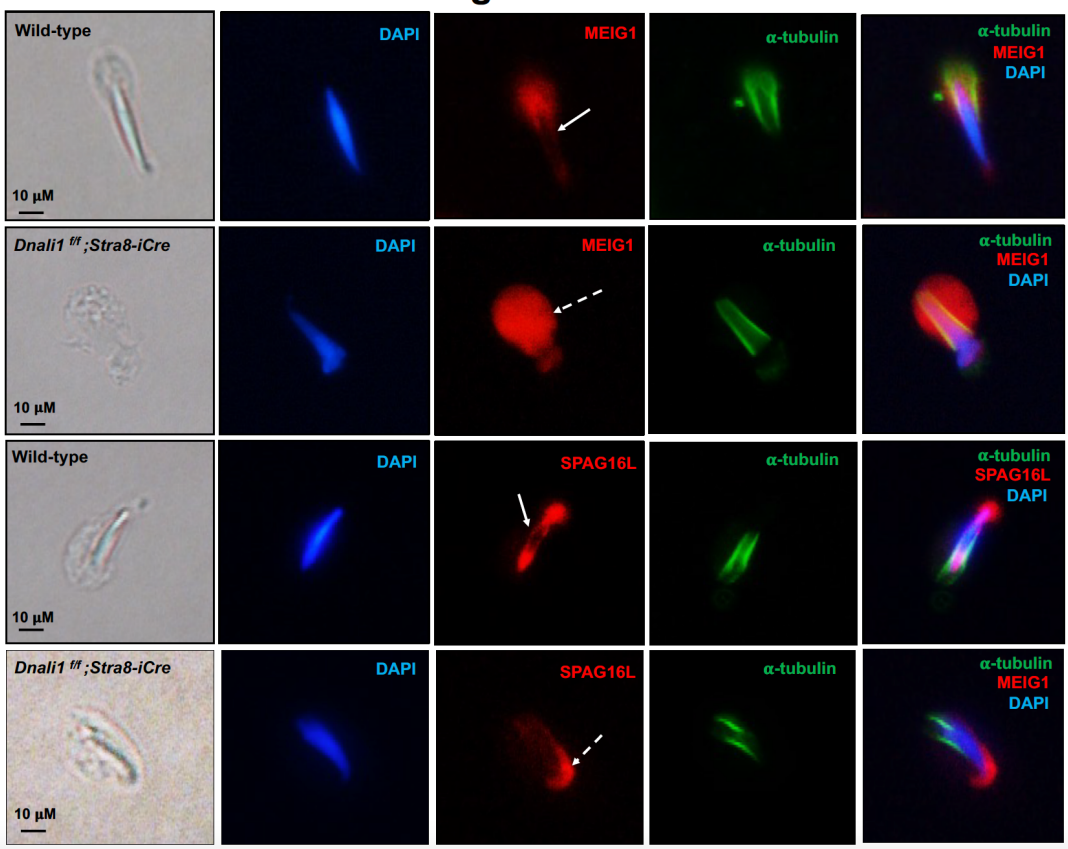


547

548 **Figure 9. Expression levels and localization of DNALI1 downstream proteins in the**
549 ***Dnali1* cKO mice.**

550 A. Analysis of testicular expression of MEIG1, PACRG and SPAG16L in control and *Dnali1*
551 cKO mice by Western blot. Compared with control mice, there was no significant change in
552 the expression level of these three proteins in the *Dnali1* cKO mice. a. Representative Western
553 blot results; b. Statistical analysis of the protein levels normalized by β-actin. n=4.

554 B. Localization of MEIG1 in spermatocytes and round spermatids of the control and *Dnali1*
555 cKO mice by immunofluorescence staining. There is no difference between the control and the
556 *Dnali1* cKO: MEIG1 is present in cell bodies in both genotypes.

557 C. Localization of SPAG16L in spermatocytes and round spermatids of the control and *Dnali1*
558 cKO mice by immunofluorescence staining. There is no difference between the control and the
559 *Dnali1* cKO: SPAG16L is present in cell bodies in both genotypes. The white dashed arrow
560 points to an elongating spermatid, and the SPAG16L is present in the manchette.

561 D. Localization of MEIG1 and SPAG16L in elongating spermatids of the control and *Dnali1*
562 cKO mice. Both MEIG1 and SPAG16L are present in the manchette in the control mice (white
563 arrows); however, they are no longer present in the manchette in the *Dnali1* cKO mice (dashed
564 white arrows).

565 (Images taken with a Nikon DS-Fi2 Eclipse 90i Motorized Upright Fluorescence Microscope).

566

567 **Discussion**

568 The *Parcg* gene is a reverse strand gene located upstream of the *Parkin* gene, involved in
569 Parkinson's disease (34). Genetic disruption of *Pacrg* in mouse phenocopies the infertility
570 phenotype of *Meig1* knockout mice (27, 29, 35-38). Our previous studies demonstrated that
571 MEIG1 and PACRG form a complex in the manchette for protein cargo transport to build the
572 sperm flagellum. We further discovered that four amino acids on the same surface of MEIG1
573 protein are involved in its interaction with PACRG (28, 29). However, it was not clear how the
574 MEIG1/PACRG complex associates with the manchette microtubules. Given that MEIG1 is a
575 downstream binding partner of PACRG, and the fact that PACRG does not associate with
576 microtubules directly, we hypothesized that there must be other upstream players involved in
577 the manchette localization of the MEIG1/PACRG complex. Therefore, we performed a yeast
578 two-hybrid screen using a PACRG component as bait. Besides MEIG1, DNALI1 was
579 identified to be major binding partner. The interaction between PACRG and DNALI1 was
580 further confirmed by other experiments described in this study, including the gel filtration and
581 protein complementation experiments.

582 The functional assays reported here also support the observed interaction between PACRG and
583 DNALI1. Previously, we discovered that mouse PACRG was not stable but could be stabilized
584 by MEIG1 in both bacteria and mammalian cells (28). The studies here showed that DNALI1
585 also stabilized PACRG, suggesting a dual association of PACRG with MEIG1 and DNALI1.
586 Similar to the MEIG1 protein, co-expression of DNALI1 also prevented degradation of
587 PACRG in both bacteria and mammalian cells, which is consistent with the reported regulation
588 of PACRG by the ubiquitin-proteasomal system (UPS) (39). It is possible that the binding site
589 on the PACRG recognized by the UPS system is protected by DNALI1, providing PACRG
590 protein more stability.
591
592 This association between PACRG and DNALI1 was also supported by *in vivo* studies. During
593 the first wave of spermatogenesis, expression of the DNALI1 protein was dramatically
594 increased during the spermiogenesis phase, which was similar to the PACRG protein (22, 28)
595 and specific to the period of spermatid elongation and formation of flagella. However, prior to
596 spermiogenesis, in late meiotic germ cells, the DNALI1 signal was weak (22). In elongating
597 spermatids, DNALI1 was localized in the manchette, coinciding with the localization of
598 PACRG, which strongly suggested that DNALI1 would have a function related to that of
599 PACRG. Testing this hypothesis through the use of conditional *Dnali1* knockout mice revealed
600 a co-dependence between the two proteins for structural integrity of spermatid elongation, the
601 absence of which leads to abnormal sperm morphology, immotility and complete male
602 infertility.

It is not surprising to see dramatically reduced sperm counts associated with impaired spermiogenesis, because DNALI1 forms a complex with MEIG1/PACRG. Disruption of either *Meig1* or *Pacrg* in the male germ cells resulted in a similar phenotype of impaired spermiogenesis and male infertility (26, 27, 34-38). The manchette is believed to play an important role in transporting cargo proteins for the formation of sperm flagella, and the transport function needs motor proteins (30, 40). Several motor proteins have been reported to be present in the manchette (41-44), and some have been shown to be essential for flagella formation (45, 46). It is highly possible that DNALI1 is the major driving force in transporting the MEIG1/PACRG complex together with the sperm flagellar proteins, including SPAG16L, along the manchette microtubules in order to assemble a functional sperm tail. It appears that DNALI1 is an upstream protein of MEIG1/PACRG complex, because DNALI1 is still in the manchette when PACRG is absent **(Figure 10A)**. In the absence of DNALI1, MEIG1 and the cargo protein SPAG16L are no longer present in the manchette. As a light chain protein, it is unlikely that DNALI1 binds directly to the manchette microtubules, based on its localization in the transfected mammalian cells. However, DNALI1 has been reported to be a binding partner of dynein heavy chain 1 protein (DYNC1H1) (22) and our current study revealed evidence that the dynein heavy chain 1 protein is also present in the manchette (**Supplemental Figure 7**). Thus, it is more likely that DNALI1 associates with the manchette microtubules through dynein heavy chain 1. Another function of the manchette is to help shape the head of developing spermatids (47, 48). Like the *Meig1* and *Pacrg* mutant mice, the *Dnali1* cKO mice

624 also developed abnormal sperm heads, which further supports the claim that DNALI1 is
625 involved in the construction of a functional manchette.
626
627 Formation of the flagellum involves both the IMT and the IFT and the complex abnormal sperm
628 phenotype observed in the *Dnali1* cKO appears to be due to the disruption of both pathways.
629 The IMT mediates the transport of cargo proteins to the basal bodies, the template and the start
630 point from which the sperm axoneme is formed (30). In the *Dnali1* cKO mice, although some
631 sperm were formed, none had normal morphology. Besides abnormal heads, the flagella
632 showed multiple defects, including short tails and vesicles and gaps along the sperm tail. The
633 partial formation of the tails indicates that the IMT may not always be disrupted, possibly due
634 to an incomplete excision by the Cre recombinase, allowing for limited DNALI1 protein
635 synthesis.
636
637 The IFT is one of the more important mechanism involved in the formation of cilia/flagella
638 (49). The IFT complex is composed of core IFT components, BBSomes, the motor proteins
639 and cargo proteins (50) and the IFT transport process is bidirectional. Through antegrade
640 transport, the cargo proteins are transported from the basal bodies to the tips of cilia/flagella
641 and by the retrograde transport it is possible for the turn-over products to be transported back
642 to the cell body for recycling. The morphological abnormalities observed in cKO sperm lead
643 us to hypothesize that DNALI1 may also be involved in the intraflagellar transport (IFT)
644 process. Defects in IFT result in failure of ciliogenesis, including formation of the sperm

flagellum (51-58). Motor proteins have been shown to be essential for a functional IFT (59, 60). Therefore, given the ultrastructural abnormalities in the sperm flagella, loss of DNALI1 might also result in IFT dysfunction (**Figure 10B)**, and be a major contributing factor to sperm immotility. Although we cannot exclude the possibility that other transport systems mediate the transport of cargo proteins in the manchette, data presented here show that the MEIG1/PACRG/DNALI1 complex does transport some cargo proteins that are essential for the formation of a normal sperm tail.

TEM study revealed a disorganized fibrous sheath, sperm tail structure in the *Dnali1* cKO mice. The fibrous sheath is a cytoskeletal structure of the principal piece in the flagellum, which consists of two longitudinal columns connected by semicircular ribs. The longitudinal columns are attached to outer dense fibers 3 and 8 in the anterior part of the principal piece and replace those fibers in the middle and posterior part of the principal piece and become associated with microtubule doublets 3 and 8 (61). It is assumed that such an elaborate substructural organization of the fibrous sheath into longitudinal columns and semicircular ribs must have a function, but testable hypotheses surrounding these characteristics are lacking. In *Dnali1* mutant mice, the two longitudinal columns were not associated with microtubule doublets 3 and 8, and the two semi circumferential ribs showed defective or asymmetrical alignment in the principal piece. It is speculated that the fibrous sheath serves as a scaffold for proteins participating in glycolysis, cAMP-dependent signaling transduction and mechanical support (62, 63). The cAMP-signaling pathway has been linked to the regulation of sperm maturation,

666 motility, capacitation, hyperactivation, and the acrosome reaction (64). Therefore, defects in
667 the development and function of the fibrous sheath may also contribute to infertility of *Dnali1*
668 cKO mice. Dysfunction in IMT and IFT may contribute to these structural defects.
669
670 Another interesting phenotype observed was an occasional failure of sperm individualization,
671 or disengagement (65-67), at the late spermatid step in the *Dnali1* cKO mice. This abnormality
672 was not observed in the *Meig1* and *Pacrg* mutant mice (26, 27, 34-38). Individualization
673 defects are the most common cause of human male infertility (68). Disengagement is one of
674 the later steps of spermiogenesis, that occurs when the membrane-cytoskeleton individualized
675 complex (IC) is assembled around the nucleus of each bundle of 64 haploid elongated
676 spermatid nuclei. Each IC is composed of 64 F-actin-based investment cones, which move the
677 flagella downward as a coordinated ensemble. Each spermatid is individualized of a single
678 cone. As IC progresses, the cytoplasm is removed from the flagella, and the membrane
679 surrounding each spermatid is reshaped to form the individualized spermatozoa (69, 70). It has
680 been reported using genetic studies that at least 70 genes are involved in the process of
681 disengagement and individualization. Several molecular pathways contribute to this process,
682 including actin and microtubule dynamics, the ubiquitin-proteasome pathway components,
683 apoptotic elimination of cytoplasmic contents, plasma membrane reorganization, and the
684 formation of a disengagement complex (65, 67, 71-73). The microtubule cytoskeleton is
685 important for individualization (73). Complexes of microtubules and dynein and kinesin
686 motors form the core of cilia and flagella (74). Mutations in the components of the dynein-

687 dynein complex, including the cytoplasmic dynein intermediate chain (CDIC), the two
688 Drosophila dynein light chains DDLC1 and DLC90F, disrupt the synchronous movement of
689 actin cones, but they also disrupt the nucleus shaping and positioning (75-77). These consistent
690 phenotypes suggest that DNALI1 may have a similar effect on the synchronous movement of
691 actin cones in sperm individualization and that DNALI1 has other functions in male germ cell
692 development that differ from the MEIG1/PACRG complex (**Figure 10C**).
693
694 Another potential function of DNALI1 is its reported activity as an inner dynein arm (IDA)
695 component of the cilium and flagellum axoneme (78). This would not be surprising in sperm,
696 as it is present along the entire length of the sperm flagellar axoneme (22). Dynein proteins are
697 present in the outer (ODAs) and inner dynein arms (IDAs) of the axonemal complex, and both
698 arms are essential for the beating of cilia and flagella (78, 79). IDAs have seven major
699 subspecies and four minor subspecies (60), but little is known about the functional differences
700 between these subspecies (80-82). Therefore, if DNALI1 does serve this function in the sperm
701 axoneme, its inactivation in male germ cells would likely disrupt the function of the dynein
702 arms, and contribute to the formation of immotile sperm (**Figure 10D)**.

## Figure 10

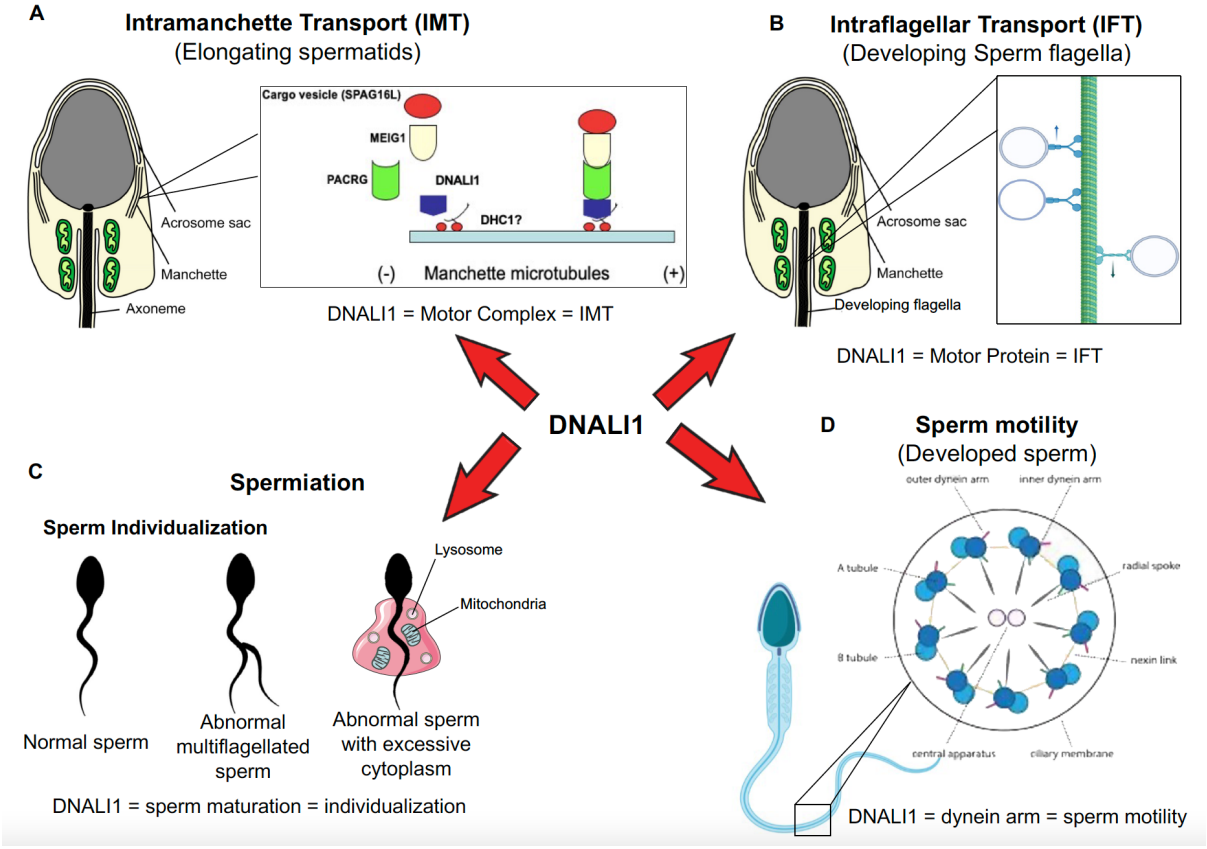


**Figure 10. Working model of DNALI1 in sperm cell differentiation and function.**

A. DNALI1 forms a complex with MEIG1/PACRG, with DNALI1 being an upstream protein that recruits downstream PACRG and MEIG1 to the manchette. DNALI1 associates with the manchette microtubules through other molecular motor protein(s), including dynein heavy chain 1. MEIG1/PACRG/DNALI1/motor complex transports cargos, including SPAG16L along the manchette to build sperm flagella.

B. DNALI1 might also function as a motor protein involved in transporting IFT particles.

C. DNALI1 may facilitate in the appropriate maturation and individualization of sperm cells.

D. DNALI1 is present in the dynein arm and functions in sperm motility.

714 In summary, DNALI1 potentially has multiple roles in sperm formation and function. We
715 demonstrated a main function in IMT but additional roles of DNALI1 are possible in IFT and
716 sperm individualization and disengagement, all of which being biological processes that occur
717 during spermiogenesis. Failure of these processes causes impaired sperm formation and
718 function and finally results in male infertility. While we show that an IMT function is clearly
719 associated with the MEIG1/PACRG complex, the potential function of DNALI1 in IFT, sperm
720 individualization and spermiation are not clear and will need further investigation.
721

722 **Acknowledgments**

723 This research was supported by Wayne State University Start-up fund and Wayne State
724 University Research Fund, MCI pilot award (to ZZ), MCI fellowship (to YTY), NIH
725 R01DK76229 (JGG) and an NIH grant R01DK115563 (to DCW). Funding was also obtained
726 from Agence Nationale pour la Recherche (grant FLAGELOME ANR-19-CE17-0014 to
727 AT). We also thank Dr Scott C. Henderson and Frances K. White for their assistance with
728 using the confocal microscopy in Microscopy Core Facility of Virginia Commonwealth
729 University.
730

731 **Declaration of interest**

732 There is no conflict of interest that could be perceived as prejudicing the impartiality of the
733 research reported.
734

735 **References**

736 1. Dutcher, S.K. Flagellar assembly in two hundred and fifty easy-to-follow steps. *Trends*
737 *Genet.* **1995**, *11 (10)*, pp. 398-404.

738 2. Ibanez-Tallon, I.; Gorokhova, S.; Heintz, N. Loss of function of axonemal dynein Mdnah5
739 causes primary ciliary dyskinesia and hydrocephalus. *Hum Mol Genet*. **2002**, *11 (6)*, pp. 715-
740 21.

741 3. Neesen, J.; Drenckhahn, J.D.; Tiede, S.; Burfeind, P.; Grzmil, M.; Konietzko, J.; Dixkens,
742 C.; Kreutzberger, J.; Laccone, F.; Omran, H. Identification of the human ortholog of the t-
743 complex-encoded protein TCTE3 and evaluation as a candidate gene for primary ciliary
744 dyskinesia. *Cytogenet Genome Res.* **2002**, *98 (1)*, pp. 38-44.

745 4. Leigh, M.W.; Pittman, J.E.; Carson, J.L.; Ferkol, T.W.; Dell, S.D.; Davis, S.D.; Knowles,
746 M.R.; Zariwala, M.A. Clinical and genetic aspects of primary ciliary dyskinesia/Kartagener
747 syndrome. *Genet Med*. **2009**, *11(7)*, pp. 473-87.

748 5. Noone, P.G.; Leigh, M.W.; Sannuti, A.; Minnix, S.L.; Carson, J.L.; Hazucha, M.; Zariwala,
749 M.A.; Knowles, M.R. Primary ciliary dyskinesia: diagnostic and phenotypic features. *Am J*
750 *Respir Crit Care Med*. **2004**, *169 (4)*, pp. 459-67.

751 6. Gibbons, I.R. Dynein family of motor proteins: present status and future questions. *Cell*
752 *Motil Cytoskeleton*. **1995**, *32 (2)*, pp. 136-44.

753 7. King, S.M. The dynein microtubule motor. *Biochim Biophys Acta.* **2000**, *1496 (1)*, pp. 60-
754 75.

755 8. Neesen, J.; Kirschner, R.; Ochs, M.; Schmiedl, A.; Habermann, B.; Mueller, C.; Holstein,
756 A.F.; Nuesslein, T.; Adham, I.; Engel, W. Disruption of an inner arm dynein heavy chain gene
757 results in asthenozoospermia and reduced ciliary beat frequency. *Hum Mol Genet*. **2001**, *10*
758 *(11)*, pp. 1117-28.
759 9. Supp, D.M.; Witte, D.P.; Potter, S.S.; Brueckner, M. Mutation of an axonemal dynein affects
760 left-right asymmetry in inversus viscerum mice. *Nature*. **1997**, *389 (6654)*, pp. 963-6.
761 10. LeDizet, M.; Piperno, G. ida4-1, ida4-2, and ida4-3 are intron splicing mutations affecting
762 the locus encoding p28, a light chain of Chlamydomonas axonemal inner dynein arms. *Mol*
763 *Biol Cell*. **1995**, *6 (6)*, pp. 713-23.
764 11. Kastury, K.; Taylor, W.E.; Shen, R.; Arver, S.; Gutierrez, M.; Fisher, C.E.; Coucke, P.J.;
765 Van Hauwe, P.; Van Camp, G.; Bhasin, S. Complementary deoxyribonucleic acid cloning and
766 characterization of a putative human axonemal dynein light chain gene. *J Clin Endocrinol*
767 *Metab*. **1997**, *82 (9)*, pp. 3047-53.
768 12. Mishra, M.; Paunesku, T.; Woloschak, G.E.; Siddique, T.; Zhu, L.J.; Lin, S.; Greco, K.;
769 Bigio, E.H. Gene expression analysis of frontotemporal lobar degeneration of the motor neuron
770 disease type with ubiquitinated inclusions. *Acta Neuropathol*. **2007**, *114 (1)*, pp. 81-94.
771 13. Loges, N.T.; Olbrich, H.; Becker-Heck, A.; Haffner, K.; Heer, A.; Reinhard, C.; Schmidts,
772 M.; Kispert, A.; Zariwala, M.A.; Leigh, M.W.; Knowles, M.R.; Zentgraf, H.; Seithe, H.;
773 Nurnberg, G.; Nurnberg, P.; Reinhardt, R.; Omran, H. Deletions and point mutations of
774 LRRC50 cause primary ciliary dyskinesia due to dynein arm defects. *Am J Hum Genet*. **2009**,
775 *85 (6)*, pp. 883-9.

776 14. Parris, T.Z.; Danielsson, A.; Nemes, S.; Kovacs, A.; Delle, U.; Fallenius, G.; Mollerstrom,
777 E.; Karlsson, P.; Helou, K. Clinical implications of gene dosage and gene expression patterns
778 in diploid breast carcinoma. *Clin Cancer Res*. **2010**, *16 (15)*, pp. 3860-74.
779 15. Tian, W.; Li, Y.; Zhang, J.; Li, J.; Gao, J. Combined analysis of DNA methylation and gene
780 expression profiles of osteosarcoma identified several prognosis signatures. *Gene*. **2018**, *650*,
781 pp. 7-14.
782 16. Peng, Y.; Chen, Z.; Guan, W.J.; Zhu, Z.; Tan, K.S.; Hong, H.; Zi, X.; Zeng, J.; Li, Y.; Ong,
783 Y.K.; Thong, M.; Shi, L.; Yang, Q.; Qiu, Q.; Wang, D.Y. Downregulation and Aberrant
784 Localization of Forkhead Box J1 in Allergic Nasal Mucosa. *Int Arch Allergy Immunol.* **2018**,
785 *176 (2)*, pp. 115-23.
786 17. Ye, Z.; Wang, F.; Yan, F.; Wang, L.; Li, B.; Liu, T.; Hu, F.; Jiang, M.; Li, W.; Fu, Z.
787 Bioinformatic identification of candidate biomarkers and related transcription factors in
788 nasopharyngeal carcinoma. *World J Surg Oncol*. **2019**, *17 (1)*, pp. 60.
789 18. Piras, I.S.; Krate, J.; Delvaux, E.; Nolz, J.; Mastroeni, D.F.; Persico, A.M.; Jepsen, W.M.;
790 Beach, T.G.; Huentelman, M.J.; Coleman, P.D. Transcriptome Changes in the Alzheimer's
791 Disease Middle Temporal Gyrus: Importance of RNA Metabolism and Mitochondria-
792 Associated Membrane Genes. *J Alzheimers Dis*. **2019**, *70 (3)*, pp. 691-713.
793 19. Wang, T.; Zhu, W.; Zhang, H.; Wen, X.; Yin, S.; Jia, Y. Integrated analysis of proteomics
794 and metabolomics reveals the potential sex determination mechanism in Odontobutis
795 potamophila. *J Proteomics*. **2019**, *208*, pp. 103482.

796 20. Pan, Z.; Zhu, C.; Chang, G.; Wu, N.; Ding, H.; Wang, H. Differential expression analysis
797 and identification of sex-related genes by gonad transcriptome sequencing in estradiol-treated
798 and non-treated Ussuri catfish Pseudobagrus ussuriensis. *Fish Physiol Biochem*. **2021**, *47 (2)*,
799 pp. 565-81.
800 21. Wang, L.; Tan, X.; Zou, C.; Wang, L.; Wu, Z.; Zou, Y.; Song, Z.; You, F. Sexually
801 dimorphic expression and regulatory sequence of dnali1 in the olive flounder Paralichthys
802 olivaceus. *Mol Biol Rep*. **2021**, *48 (4)*, pp. 3529-40.
803 22. Rashid, S.; Breckle, R.; Hupe, M.; Geisler, S.; Doerwald, N.; Neesen, J. The murine Dnali1
804 gene encodes a flagellar protein that interacts with the cytoplasmic dynein heavy chain 1. *Mol*
805 *Reprod Dev*. **2006**, *73 (6)*, pp. 784-94.
806 23. Hecht, N.B. Molecular mechanisms of male germ cell differentiation. *Bioessays.* **1998**, *20*
807 *(7)*, pp. 555-61.
808 24. Pleuger, C.; Lehti, M.S.; Dunleavy, J.E.; Fietz, D.; O'Bryan, M.K. Haploid male germ cells-
809 the **Grand** Central Station of protein transport. *Hum Reprod Update*. **2020,** *26 (4)*, pp. 474-
810 500.
811 25. Yan, W. Male infertility caused by spermiogenic defects: lessons from gene knockouts.
812 *Mol Cell Endocrinol*. **2009**, *306 (1-2)*, pp. 24-32.
813 26. Zhang, Z.; Shen, X.; Gude, D.; Wilkinson, B.K.; Justice, M.J.; Flickinger, C.J.; Herr, J.C.;
814 Eddy, E.M.; Strauss, J.F. MEIG1 is essential for spermiogenesis in mice. *Proc Natl Acad Sci*
815 *USA*. **2009**, *106 (40)*, pp. 17055-60.

816 27. Li, W.; Tang, W.; Teves, M.E.; Zhang, Z.; Zhang, L.; Li, H.; Archer, K.J.; Peterson, D.L.;
817 Williams, D.C.; Strauss, J.F.; Zhang, Z. A MEIG1/PACRG complex in the manchette is
818 essential for building the sperm flagella. *Development*. **2015**, *142 (5)*, pp. 921-30.
819 28. Li, W.; Walavalkar, N.M.; Buchwald, W.A.; Teves, M.E.; Zhang, L.; Liu, H.; Bilinovich,
820 S.; Peterson, D.L.; Strauss, J.F.; Williams, D.C.; Zhang, Z. Dissecting the structural basis of
821 MEIG1 interaction with PACRG. *Sci Rep*. **2016**, *6*, pp. 18278.
822 29. Li, W.; Huang, Q.; Zhang, L.; Liu, H.; Zhang, D.; Yuan, S.; Yap, Y.T.; Qu, W.; Shiang, R.;
823 Song, S.; Hess, R.A.; Zhang, Z. A single amino acid mutation in the mouse MEIG1 protein
824 disrupts a cargo transport system necessary for sperm formation. *J Biol Chem.* **2021**. *297 (5)*,
825 pp. 101312.
826 30. Kierszenbaum, A.L. Intramanchette transport (IMT): managing the making of the
827 spermatid head, centrosome, and tail. *Mol Reprod Dev*. **2002**, *63 (1)*, pp. 1-4.
828 31. Huang, Q.; Li, W.; Zhou, Q.; Awasthi, P.; Cazin, C.; Yap, Y.; Mladenovic-Lucas, L.; Hu,
829 B.; Jeyasuria, P.; Zhang, L.; Granneman, J.G.; Hess, R.A.; Ray, P.F.; Kherraf, Z.E.; Natarajan,
830 V.; Zhang, Z. Leucine zipper transcription factor-like 1 (LZTFL1), an intraflagellar transporter
831 protein 27 (IFT27) associated protein, is required for normal sperm function and male fertility.
832 *Dev Biol*. **2021**, *477*, pp. 164-176.
833 32. Sadate-Ngatchou, P.I.; Payne, C.J.; Dearth, A.T.; Braun, R.E. Cre recombinase activity
834 specific to postnatal, premeiotic male germ cells in transgenic mice. *Genesis.* **2008**, *46 (12)*,
835 738-42.

836 33. Lores et al. Mutations in TTC29, Encoding an Evolutionarily Conserved Axonemal
837 Protein, Result in Asthenozoospermia and Male Infertility. *Am J Hum Genet.* **2019**, 105(6),
838 1148-1167.
839 34. West, A.B.; Lockhart, P.J.; O'Farell, C.; Farrer, M.J. Identification of a novel gene linked
840 to parkin via a bi-directional promoter. *J Mol Biol*. **2003**, *326 (1)*, pp. 11-9.
841 35. Bennett, W.I.; Gall, A.M.; Southard, J.L.; Sidman, R.L. Abnormal spermiogenesis in
842 quaking, a myelin-deficient mutant mouse. *Biol Reprod*. **1971**, *5 (1),* pp. 30-58.
843 36. Lockhart, P.J.; O'Farrell, C.A.; Farrer, M.J. It's a double knock-out! The quaking mouse is
844 a spontaneous deletion of parkin and parkin co-regulated gene (PACRG). *Mov Disord.* **2004**,
845 *19 (1),* pp. 101-4.
846 37. Lorenzetti, D.; Bishop, C.E.; Justice, M.J. Deletion of the Parkin coregulated gene causes
847 male sterility in the quaking(viable) mouse mutant. *Proc Natl Acad Sci USA*. **2004**, *101 (22)*,
848 pp. 8402-7.
849 38. Stephenson, S.E.M.; Aumann, T.D.; Taylor, J.M.; Riseley, J.R.; Li, R.; Mann, J.R.; Tomas,
850 D.; Lockhart, P.J. Generation and characterisation of a parkin-Pacrg knockout mouse line and
851 a Pacrg knockout mouse line. *Sci Rep*. **2018**, *8 (1)*, pp. 7528.
852 39. Taylor, J.M.; Brody, K.M.; Lockhart, P.J. Parkin co-regulated gene is involved in
853 aggresome formation and autophagy in response to proteasomal impairment. *Exp Cell Res*.
854 **2012**, *318 (16),* pp. 2059-70.
855 40. Lehti, M.S.; Sironen, A.Formation and function of the manchette and flagellum during
856 spermatogenesis. *Reproduction.* **2016,** *151 (4)*, pp. R43-54.

857 41. Kierszenbaum, A.L.; Rivkin, E.; Tres, L.L. The actin-based motor myosin Va is a
858 component of the acroplaxome, an acrosome-nuclear envelope junctional plate, and
859 of manchette-associated vesicles. *Cytogenet Genome Res*. **2003,** *103 (3-4)*, pp. 337-44.
860 42. Yang, W.X.; Jefferson, H.; Sperry, A.O. The molecular motor KIFC1 associates with a
861 complex containing nucleoporin NUP62 that is regulated during development and by the small
862 GTPase RAN. *Biol Reprod.* **2006**, *74 (4)*, pp. 684-90.
863 43. Hayasaka, S.; Terada, Y.; Suzuki, K.; Murakawa, H.; Tachibana, I.; Sankai, T.; Murakami,
864 T.; Yaegashi, N.; Okamura, K. Intramanchette transport during primate spermiogenesis:
865 expression of dynein, myosin Va, motor recruiter myosin Va, VIIa-Rab27a/b
866 interacting protein, and Rab27b in the manchette during human and monkey spermiogenesis.
867 *Asian J Androl*. **2008**, *10 (4)*, pp. 561-8.
868 44. Saade, M.; Irla, M.; Govin, J.; Victorero, G.; Samson, M.; Nguyen, C. Dynamic distribution
869 of Spatial during mouse spermatogenesis and its interaction with the kinesin KIF17b. *Exp Cell*
870 *Res.* **2007**, *313 (3)*, pp. 614-26.
871 45, Lehti, M.S.; Kotaja, N.; Sironen, A. KIF3A is essential for sperm tail formation
872 and manchette function. *Mol Cell Endocrinol.* **2013**, *377 (1-2)*, pp. 44-55.
873 46. Christman, D.A.; Curry, H.N.; Rouhana, L. Heterotrimeric Kinesin II is required for
874 flagellar assembly and elongation of nuclear morphology during spermiogenesis in Schmidtea
875 mediterranea. *Dev Biol.* **2021**, *477*, pp. 191-204.
876 47. Kierszenbaum, A.L.; Tres, L.L. The acrosome-acroplaxome-manchette complex and the
877 shaping of the spermatid head. *Arch Histol Cytol.* **2004**, *67 (4),* pp. 271-84.

878 48. Manfrevola, F.; Guillou, F.; Fasano, S.; Pierantoni, R.; Chianese, R. LINCking the Nuclear
879 Envelope to Sperm Architecture. *Genes (Basel)*. **2021**, *12 (5)*, pp.658.
880 49. Rosenbaum, J.L.; Witman, G.B. Intraflagellar transport. *Nat Rev Mol Cell Biol.* **2002**, *3*
881 *(11)*, pp. 813-25.
882 50. Prevo, B.; Scholey, J.M.; Peterman, E.J.G. Intraflagellar transport: mechanisms of motor
883 action, cooperation, and cargo delivery. *FEBS J*. **2017**, *284 (18)*, pp. 2905-2931.
884 51. Pazour, G.J.; Rosenbaum, J.L. Intraflagellar transport and cilia-dependent diseases. *Trends*
885 *Cell Biol*. **2002**, *12 (12),* pp. 551-5.
886 52. Zhang, Z.; Li, W.; Zhang, Y.; Zhang, L.; Teves, M. E.; Liu, H.; Strauss, J. F., 3rd; Pazour,
887 G. J.; Foster, J. A.; Hess, R. A.; & Zhang, Z. Intraflagellar transport protein IFT20 is essential
888 for male fertility and spermiogenesis in mice. *Mol Biol Cell*. **2016,** *27 (23)*, pp. 3705–3716.
889 53. Liu H, Li W, Zhang Y, Zhang Z, Shang X, Zhang L, Zhang S, Li Y, Somoza AV, Delpi B,
890 Gerton GL, Foster JA, Hess RA, Pazour GJ, Zhang Z. IFT25, an intraflagellar transporter
891 protein dispensable for ciliogenesis in somatic cells, is essential for sperm flagella formation.
892 *Biol Reprod.* **2017,** *96 (5)*, pp. 993-1006.
893 54. Zhang, Y.; Liu, H.; Li, W.; Zhang, Z.; Shang, X.; Zhang, D.; Li, Y.; Zhang, S.; Liu, J.;
894 Hess, R.A.; Pazour, G.J.; Zhang, Z. Intraflagellar transporter protein (IFT27), an IFT25 binding
895 partner, is essential for male fertility and spermiogenesis in mice. *Dev Biol.* **2017**, *432 (1)*, pp.
896 125-139.

897 55. Shi L, Zhou T, Huang Q, Zhang S, Li W, Zhang L, Hess RA, Pazour GJ, Zhang Z.
898 Intraflagellar transport protein 74 is essential for spermatogenesis and male fertility in mice†.
899 *Biol Reprod.* **2019**, *101 (1)*, pp. 188-199.
900 56. Qu, W., Yuan, S., Quan, C., Huang, Q., Zhou, Q., Yap, Y., Shi, L., Zhang, D., Guest, T.,
901 Li, W., Yee, S. P., Zhang, L., Cazin, C., Hess, R. A., Ray, P. F., Kherraf, Z. E., & Zhang, Z.
902 The essential role of intraflagellar transport protein IFT81 in male mice spermiogenesis and
903 fertility. *Am J Physiol Cell Physiol*. **2020**, *318 (6)*, pp. C1092-C1106.
904 57. Zhang, Y., Liu, H., Li, W., Zhang, Z., Zhang, S., Teves, M. E., Stevens, C., Foster, J. A.,
905 Campbell, G. E., Windle, J. J., Hess, R. A., Pazour, G. J., & Zhang, Z. Intraflagellar transporter
906 protein 140 (IFT140), a component of IFT-A complex, is essential for male fertility and
907 spermiogenesis in mice. *Cytoskeleton (Hoboken)*. **2018**, *75 (2)*, pp. 70-84.
908 58. Zhang, S., Liu, Y., Huang, Q., Yuan, S., Liu, H., Shi, L., Yap, Y. T., Li, W., Zhen, J., Zhang,
909 L., Hess, R. A., & Zhang, Z. Murine germ cell-specific disruption of Ift172 causes defects in
910 spermiogenesis and male fertility. *Reproduction*. **2020**, *159 (4)*, pp. 409-421.
911 59. Scholey, J.M. Kinesin-2: a family of heterotrimeric and homodimeric motors with diverse
912 intracellular transport functions. *Annu Rev Cell Dev Biol.* **2013**, *29,* pp. 443-69.
913 60. Scholey, J.M. Intraflagellar transport motors in cilia: moving along the cell's antenna. *J*
914 *Cell Biol.* **2008**, *180 (1)*, pp. 23-9.
915 61. Fawcett, D.W. The mammalian spermatozoon. *Dev Biol*. **1975**, *44 (2)*, pp. 394-436.
916 62. Eddy, E.M. The scaffold role of the fibrous sheath. *Soc Reprod Fertil Suppl*. **2007**, *65*, pp.
917 45-62.

63. Miki, K.; Qu, W.; Goulding, E.H.; Willis, W.D.; Bunch, D.O.; Strader, L.F.; Perreault, S.D.; Eddy, E.M.; O'Brien, D.A. Glyceraldehyde 3-phosphate dehydrogenase-S, a sperm-specific glycolytic enzyme, is required for sperm motility and male fertility. *Proc Natl Acad Sci USA*. **2004**, *101 (47)*, pp. 16501-6.

64. Somlyo, A.P.; Somlyo, A.V. Signal transduction by G-proteins, rho-kinase and protein phosphatase to smooth muscle and non-muscle myosin II. *J Physiol.* **2000**, *522 Pt 2*, pp. 177-85.

65. O'Donnell, L.; and Stanton, P.G. Spermiation. In: Skinner, M.L, editor. Spermiation. Encyclopedia of Reproduction (Second Edition). Oxford, United Kingdom: Academic Press**; 2018,** pp. 145-151.

66.Mäkelä, J.A.; and Toppari, J. Spermatogenic Cell Syncytium. In: Skinner, M.K., editor. Encyclopedia of Reproduction (Second Edition). Oxford, United Kingdom: Academic Press**; 2018,** pp. 124-133.

67. Hess, R.A.; and Vogl, A.W. Sertoli cell anatomy and cytoskeleton. In: Griswold, M., editor. Sertoli Cell Biology. Oxford, United Kingdom: Elsevier Academic Press**; 2015,** pp. 1-55.

68. Cooper, T.G. Cytoplasmic droplets: the good, the bad or just confusing? *Hum Reprod*. **2005**, *20 (1)*, pp. 9-11.

69. O'Donnell, L.; Nicholls, P.K.; O'Bryan, M.K.; McLachlan, R.I.; Stanton, P.G. Spermiation: The process of sperm release. *Spermatogenesis*. **2011**, *1 (1)*, pp. 14-35.

70. Tokuyasu, K.T.; Peacock, W.J.; Hardy, R.W. Dynamics of spermiogenesis in Drosophila melanogaster. I. Individualization process. *Z Zellforsch Mikrosk Anat.* **1972**, *124 (4)*, pp. 479-506.

939 71. Steinhauer, J. Separating from the pack: Molecular mechanisms of Drosophila spermatid
940 individualization. *Spermatogenesis*. **2015**, *5 (2)*, e1041345.
941 72. Zhong, L.; Belote, J.M. The testis-specific proteasome subunit Prosalpha6T of D.
942 melanogaster is required for individualization and nuclear maturation during spermatogenesis.
943 *Development*. **2007**, *134 (19)*, pp. 3517-25.
944 73. Chen, H.; Jiang, Y.; Mruk, D.D.; and Cheng, C.Y. Spermiation: Insights from Studies on the
945 Adjudin Model. *Adv Exp Med Biol.* **2021**, *1288*, pp. 241-254.
946 74. Sweeney, H.L.; Holzbaur, E.L.F. Motor Proteins. *Cold Spring Harb Perspect Biol*. **2018,**
947 *10 (5)*, a021931.
948 75. Ghosh-Roy, A.; Desai, B.S.; Ray, K. Dynein light chain 1 regulates dynamin-mediated F-
949 actin assembly during sperm individualization in Drosophila. Mol Biol Cell. 2005, 16 (7), pp.
950 3107-16.
951 76. Ghosh-Roy, A.; Kulkarni, M.; Kumar, V.; Shirolikar, S.; Ray, K. Cytoplasmic dynein-
952 dynactin complex is required for spermatid growth but not axoneme assembly in Drosophila.
953 *Mol Biol Cell.* **2004**, *15 (5)*, pp. 2470-83.
954 77. Li, M.G.; Serr, M.; Newman, E.A.; Hays, T.S. The Drosophila tctex-1 light chain is
955 dispensable for essential cytoplasmic dynein functions but is required during spermatid
956 differentiation. *Mol Biol Cell.* **2004,** *15 (7)*, pp. 3005-14.
957 78. Kamiya, R.; Okamoto, M. A mutant of Chlamydomonas reinhardtii that lacks the flagellar
958 outer dynein arm but can swim. *J Cell Sci.* **1985**, *74*, pp. 181-91.

959 79. Mitchell, D.R.; Rosenbaum, J.L. A motile Chlamydomonas flagellar mutant that lacks outer
960 dynein arms. *J Cell Biol.* **1985**, *100 (4)*, pp. 1228-34.
961 80. Bui, K.H.; Yagi, T.; Yamamoto, R.; Kamiya, R.; Ishikawa, T. Polarity and asymmetry in
962 the arrangement of dynein and related structures in the Chlamydomonas axoneme. *J Cell Biol*.
963 **2012**, *198 (5)*, pp. 913-25.
964 81. Yagi, T.; Minoura, I.; Fujiwara, A.; Saito, R.; Yasunaga, T.; Hirono, M.; Kamiya, R. An
965 axonemal dynein particularly important for flagellar movement at high viscosity. Implications
966 from a new Chlamydomonas mutant deficient in the dynein heavy chain gene DHC9. *J Biol*
967 *Chem*. **2005**, *280 (50)*, pp. 41412-20.
968 82. Kamiya, R.; Yagi, T. Functional diversity of axonemal dyneins as assessed by in vitro and
969 in vivo motility assays of Chlamydomonas mutants. *Zoolog Sci*. **2014**, *31 (10)*, pp. 633-44.

970

971

972 **Supplemental materials and legends**

## Supplemental Figure 1A

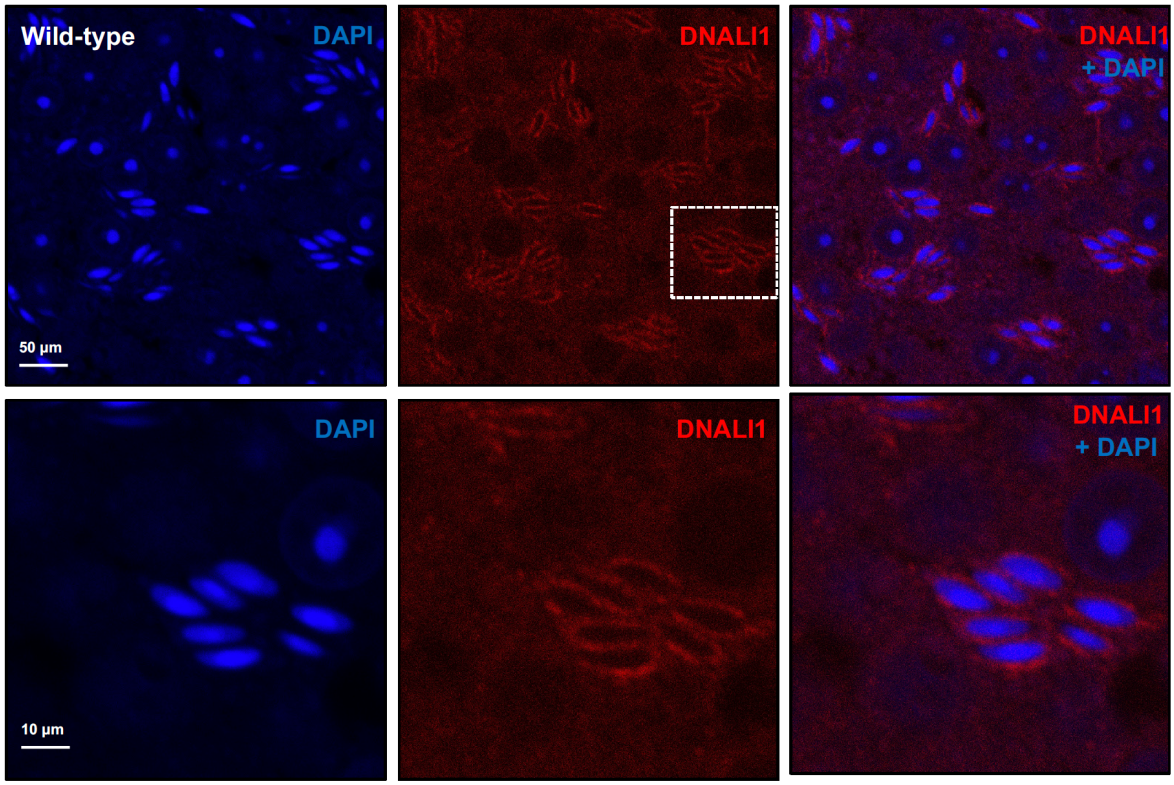


973

## Supplemental Figure 1B

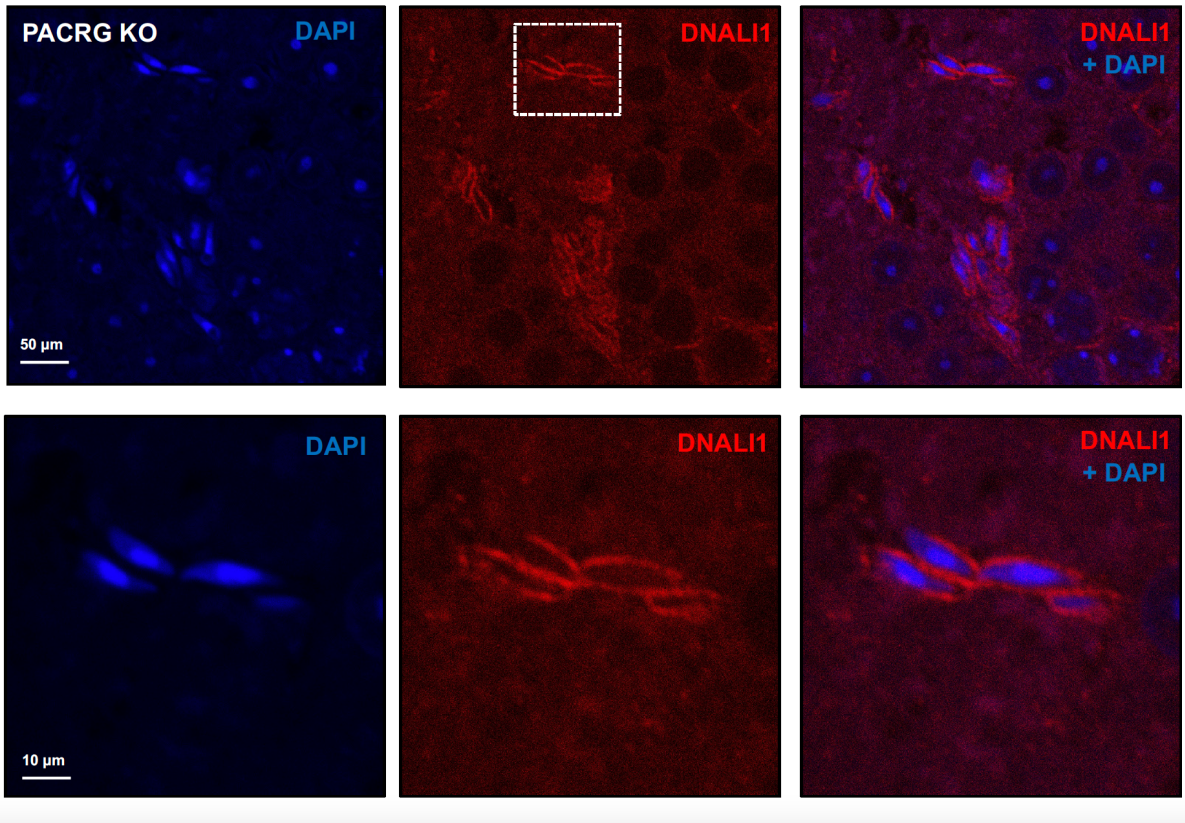


974

975 **Supplemental Figure 1. The localization of DNALI1 in the testis seminiferous tubule of a**
976 **wild-type mouse (A) and a *Pacrg* mutant mouse (B).**

977 DNALI1 was present in the manchette of elongating spermatids, and the localization was not
978 changed in the *Pacrg* mutant mice. The lower panels were the zoom-in areas from the upper
979 panels. (Images taken with confocal laser scanning microscopy (Zeiss LSM 700), Virginia
980 Commonwealth University).

## Supplemental Figure 2

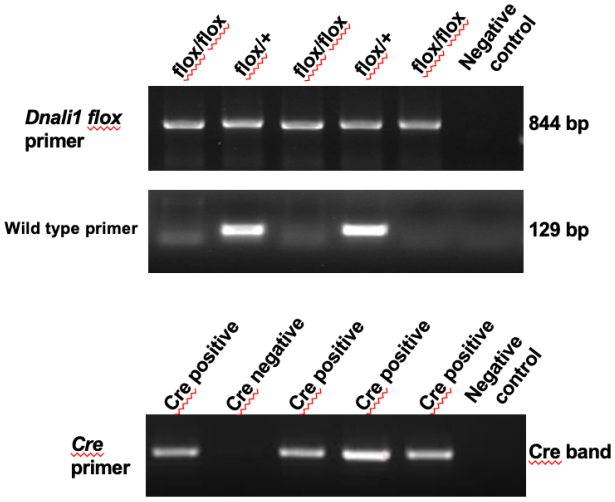


981

982 **Supplemental Figure 2. Representative PCR results showing mice with different**
983 **genotypes.**

984 Upper panel: primer set to analyze floxed *Dnali1* allele (844 bp); middle panel: primer set to
985 analyze the wild-type allele (129 bp); lower panel: primer set to detect Cre.

986

# Supplemental Figure 3

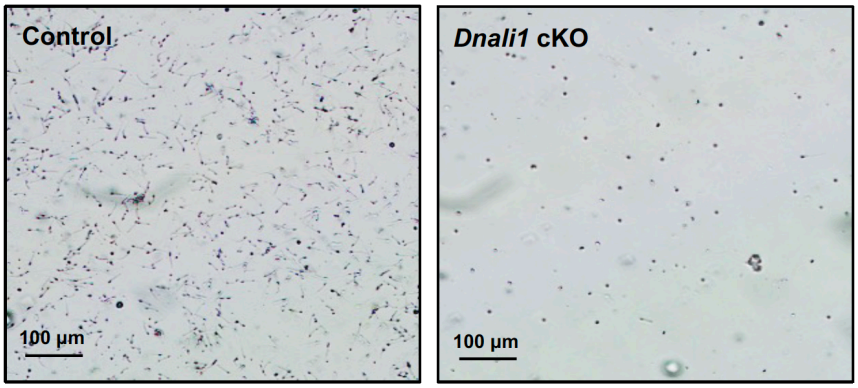


**Supplemental Figure 3. Morphological examination of epididymal sperm by light microscopy at low magnification.**

Notice that sperm density of the control mice is higher than those observed in the *Dnali1* cKO mice under the same dilution.

## Supplemental Figure 4

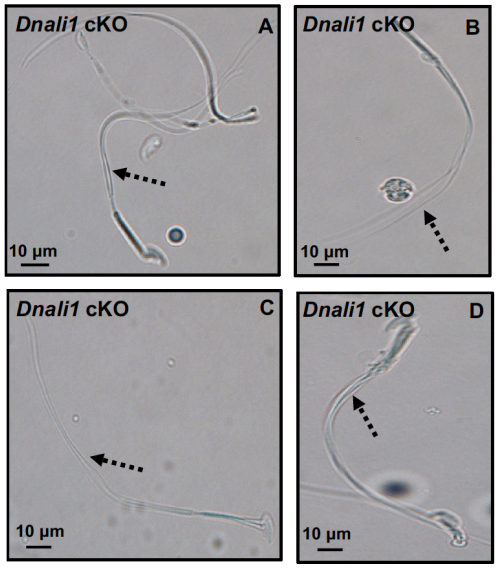


992

993 **Supplemental Figure 4. Morphological examination of epididymal sperm by light**

994 **microscopy.**

995 Multiple tails are present in the sperm (dashed arrows in A-D).

## Supplemental Figure 5A

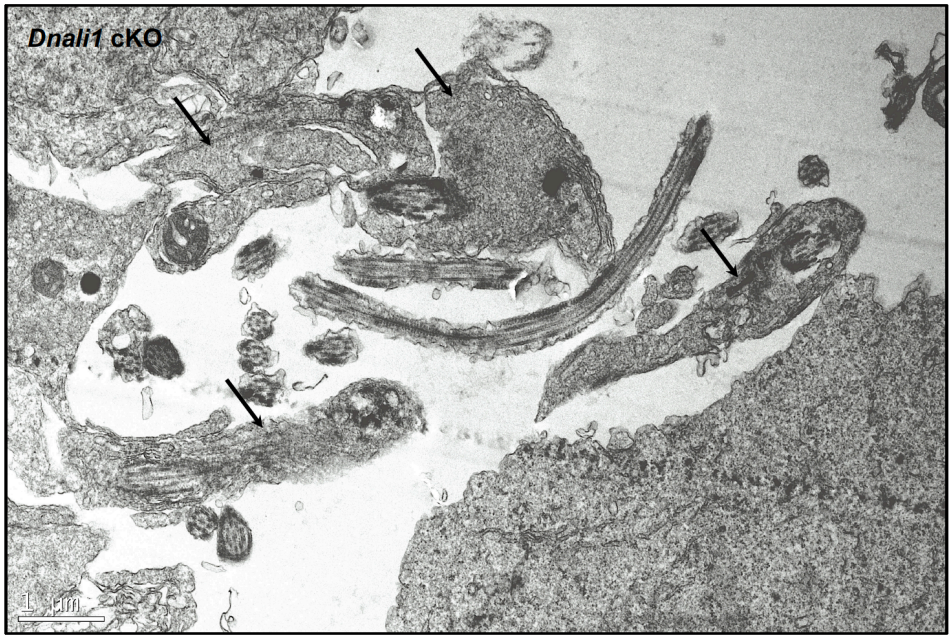


996

## Supplemental Figure 5B

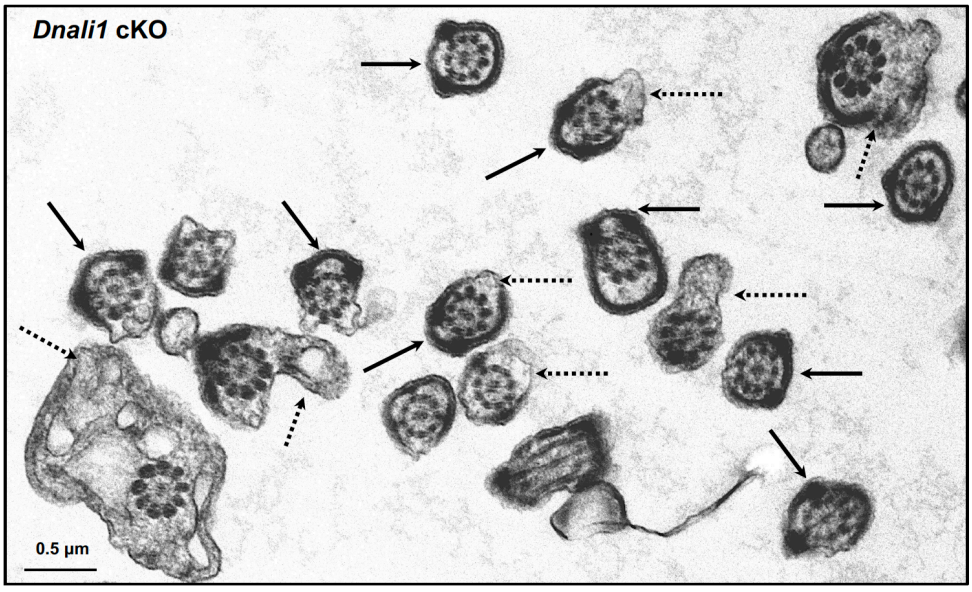


997

## Supplemental Figure 5C

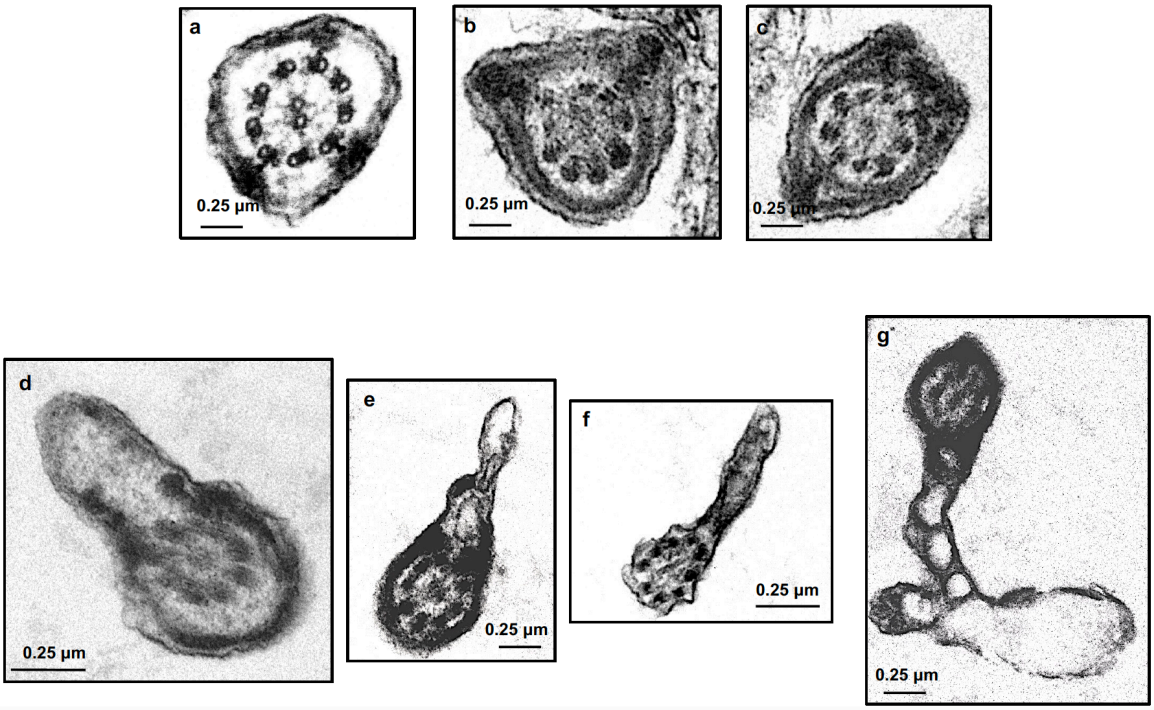


998

999 **Supplemental Figure 5. Additional testicular sperm TEM images of the *Dnali1* cKO mice.**

1000 A. Low magnification image showing retained cytoplasmic components in the lumen area

1001 (black arrows).

1002 B. Low magnification images showing abnormal fibrous sheath (black arrows) and cell

1003 membranes (dashed arrows);

1004 C. High magnification images showing abnormal fibrous sheath (a-c) and cell membranes (d-

1005 g).

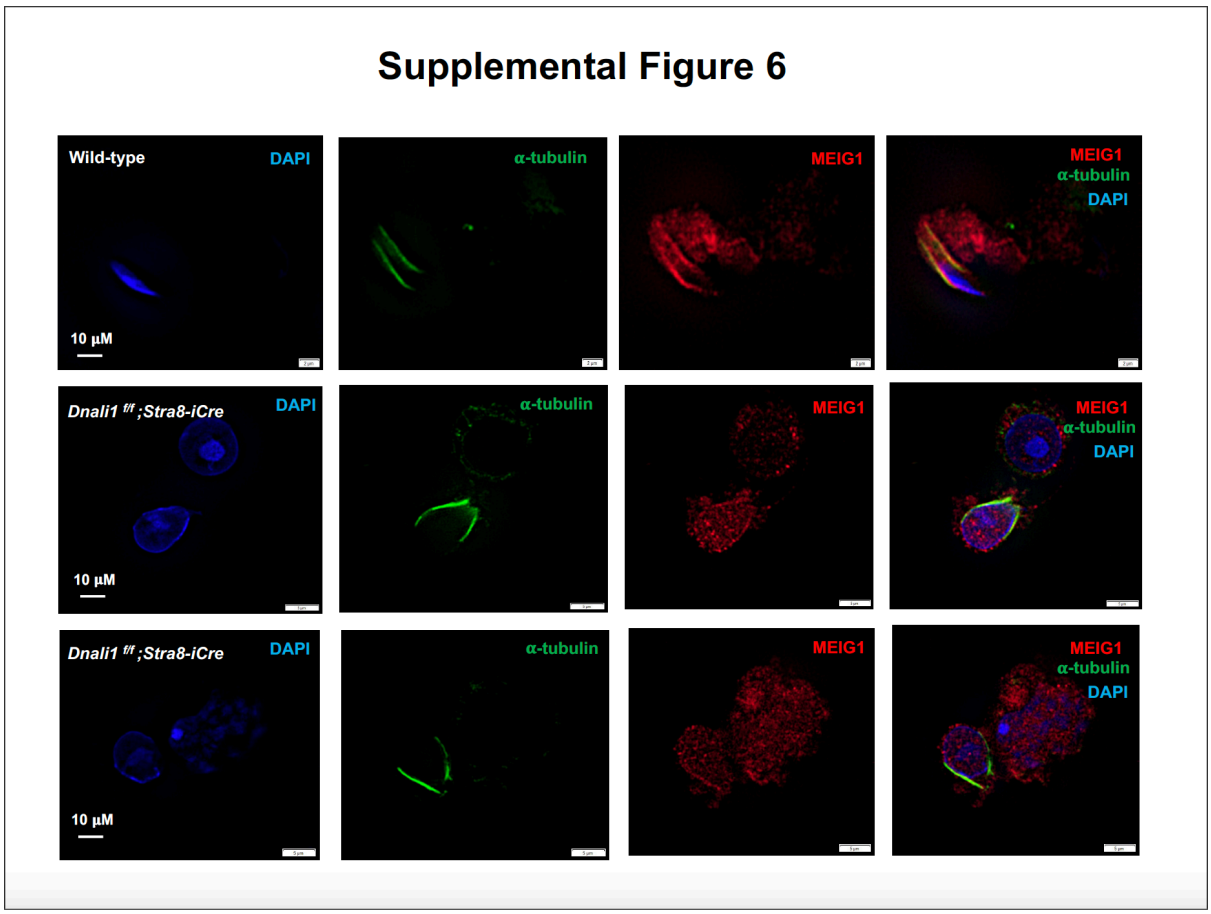


**Supplemental Figure 6. Examination of MEIG1 localization in elongating spermatids in the control and *Dnali1* cKO mice.**

Notice that MEIG1 is present in the manchette in the control mouse, but not in the *Dnali1* cKO mouse. (Images taken with Olympus IX-81 microscope equipped with a spinning-disc confocal unit (Dr. James G. Granneman's laboratory, Wayne State University).

## Supplemental Figure 7

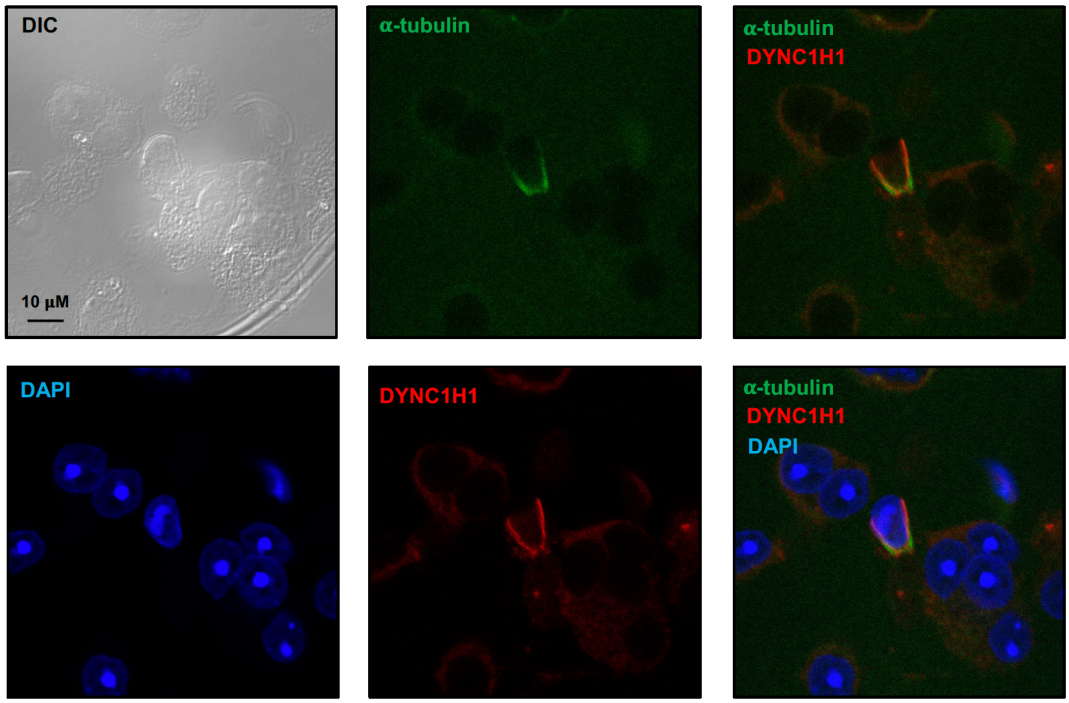


**Supplemental Figure 7. Examination of dynein heavy chain 1 protein (DYNC1H1) in male germ cells by immunofluorescence staining.**

Notice that DYNC1H1 was co-localized with α-tubulin in the elongating spermatid. (Images taken with confocal laser scanning microscopy (Zeiss LSM 700), Virginia Commonwealth University).

**Supplemental Table 1. List of putative PACRG binding proteins selected under stringent conditions.**

The full-length PACRG coding sequence was cloned into pGBKT7, which was used to screen a Mate & PlateTM Library-Universal Mouse (Normalized) (Clontech, Cat#: 630482) according to the manufacturer's instructions. The yeasts were grown on plates lacking four

1024 amino acids (Ade-Leu-His-Trp). DNALI1 was found to be one of the putative PACRG binding

1025 proteins.

1026 **List of putative PACRG binding proteins selected under stringent conditions**

| Name | NCBI number | Frequency |
|---|---|---|
| Meig1 | NM_008579 | 119 |
| Dnali1 | NM_175223 | 6 |
| Pramel42 | NM_001243938 | 3 |
| Musculus protein phosphatase 1A | BC008595 | 2 |
| Acad11 | NM_175324 | 2 |
| Ppm1a | NM_008910 | 1 |
| L2hgdh | NM_145443 | 1 |
| Tmem225 | NM_029379 | 1 |
| Tinag | NM_012033 | 1 |
| Spag6l | NM_015773 | 1 |
| Emp2 | NM_007929 | 1 |

1027

1028 **Supplemental movies**

1029 A. Representative movie from a control mouse. Note that most sperm are motile and display

1030 vigorous flagellar activity and progressive long-track forward movement.

1031 B. Representative movies from a *Dnali1* cKO mutant mouse. Notice that there are fewer sperm

1032 compared with the control mice in the same dilution, and almost all sperm are immotile.

1033